LAWRENCE
LIVERMORE
NATIONAL
LABORATORY

UCRL-TR-203891

Study of the Reactions Controlling the Mobility of Uranium in Ground and Surface Water Systems in Contact with Apatite

M. Taffet

April 30, 2004

This work was performed under the auspices of the U.S. Department of Energy by University of California, Lawrence Livermore National Laboratory under Contract W-7405-Eng-48.

TABLE OF CONTENTS

Abstract

The objective of this project was to define the mechanisms, equilibria, kinetics, and extent of sorption of aqueous uranium onto hydroxyapatite ($Ca_5(PO_4)_3(OH)$) for a range of pH, ionic strength, aqueous uranium concentration, dissolved carbon/air CO_2, and mineral surface area. We conducted chemical modeling, batch and flow-through experiments, chemical analysis, x-ray absorption and diffraction measurement, and electron microscopy. Our motivation was the need to immobilize U in water and soil to prevent it's entry into water supplies and ultimately, biological systems. Applying hydroxyapatite to in-situ treatment of uranium-bearing ground water could be an effective, low cost technology. We found that hydroxyapatite quickly, effectively, and reversibly sorbed uranium at a high capacity by inner-sphere complexation over a wide range of conditions.

Our results indicate that at aqueous uranium concentrations below 10-20 ppb: (1) equilibrium sorption of uranium to hydroxyapatite occurs in hours, regardless of pH; (2) in ambient and CO_2-free atmospheres, over 98% of initial uranium is sorbed to hydroxyapatite, (3) in waters in equilibrium with higher air CO_2 concentrations, sorption removed over 97% of aqueous uranium, except above pH 9, where aqueous uranium concentrations were reduced by less than 40%, and (4) at near-neutral pH, bicarbonate alkalinities in excess of 500 slightly retarded sorption of uranium to hydroxyapatite, relative to lower alkalinities.

Uranium sorption and precipitation are reversible and are not appreciably affected by ionic strength. The reversibility of these reactions requires that *in situ* treatment be carefully monitored to avoid breakthrough and de-sorption of uranium unto ground water.

At typical surface conditions, sorption is the only mode of uranium sequestration below 20-50 ppb U - above this range, precipitation of uranium phosphate minerals begins to dominate sequestration processes. We verified that one m^2 of hydroxyapatite can sorb over 7.53×10^{-6} moles or 1.8 mg of uranium in agreement with calculations based on phosphate and calcium oxide sites on the unit cell. Our work is significant because small masses of hydroxyapatite can sorb appreciable masses of uranium quickly over a wide range of chemistries. Preliminary work with ground water containing 260 ppb of uranium and cow bone char indicates that its sorptive capacity is appreciable less than pure hydroxyapatite. Pure crystalline hydroxyapatite sequestered 2.9 mg of uranium per m^2 as opposed to 0.083 mg of uranium sequestered per m^2 of cow bone char, or 27% versus 3.5% by surface area, respectively.

Extended x-ray adsorption fine structure (EXAFS) spectroscopy defined mono- and bidentate sorption of uranium to phosphate and calcium oxide groups on the hydroxyapatite surface. The EXAFS data indicate that up to several thousand parts U per million parts hydroxyapatite, surface complexation, and not precipitation, is the predominant process. Above this uranium: hydroxyapatite mass ratio, precipitation of meta-autunite ($H_2(UO_2)_2(PO_4)_2 \bullet 10H_20$) dominates the sequestration process.

1. Introduction

This document is the final report for Laboratory Directed Research and Development (LDRD) Project 01-ER-105. This work supports U.S. Department of Energy, National Nuclear Security Administration, and LLNL missions in Environmental Management and Environmental and Homeland Security. By providing an understanding of the mechanisms that control aqueous uranium sorption to phosphate minerals, such as hydroxyapatite, we can optimize removal of uranium from ground and surface waters, enhance filtration of uranium in drinking water and other fluids, and fixate uranium in soil and solid wastes.

Reactions between hydroxyapatite ($Ca_5(PO_4)_3(OH)$) and aqueous uranium often lead to removal of the uranium from solution. Several other metals and radionuclides exhibit similar behavior. The mechanisms and equilibria for these reactions are poorly understood. This information is important because elevated concentrations of uranium in ground water occur at many locations, including power plants, uranium enrichment, re-processing, and disposal sites and uranium mines (U.S. GAO, 1998; Abdelouas et al., 1999). Uranium is very soluble, and hence mobile, in typical surface and shallow subsurface conditions of abundant oxygen, dissolved carbon, and near-neutral pH (Langmuir, 1978 and 1997; Meinrath et al., 1999; and Burns and Finch, 1999). Aqueous uranium concentrations are limited to several ppm by the solubility of uranium minerals. Less well understood are the sorption reactions that control uranium equilibria at total concentrations below solubility controls. The low aqueous uranium concentrations (below several hundred ppb) that comprise the sorptive realm are important because they are within the range observed in typical surface- and ground waters. Thirty ppb is the Federal Maximum Contaminant Level (MCL) for total uranium in drinking water (U.S. Federal Register, 2001) and thus removing uranium at higher concentrations requires sorptive processes to satisfy the MCL. The sorption reactions between hydroxyapatite and dissolved uranium are the primary subject of this work. An understanding of these reactions can allow for efficient *in situ* treatment of uranium in a permeable reactive barrier (PRB). Hydroxyapatite can be emplaced in a PRB to passively remediate an aquifer containing a uranium plume. Additionally, these techniques could be applied in *ex-situ* uranium treatment and water filtration systems.

This research was an attempt to define the equilibrium distribution of aqueous uranium partitioned between sorbed and dissolved phases in aqueous solutions containing hydroxyapatite and its dissolution products (principally calcium and phosphate) for a range of chemical conditions typical of oxidized ground and surface waters. The work focused on pure crystalline hydroxyapatite and simple solutions containing 10^{-8} to 10^{-6} M total uranium (approximately 0.1 ppb to 15 ppb) equilibrated at initial conditions of pH 4 to 10 and aqueous uranium interaction with powdered crystalline hydroxyapatite. Some experiments were conducted at up to 10 ppm uranium. Experiments were also run with sintered amorphous hydroxyapatite, fish bone, or partially oxidized cow bone char. The goal was to better understand the chemistry involved in aqueous uranium sorption by hydroxyapatite to promote better modeling and understanding of the relevant chemical reactions in carbonate and phosphate-bearing ground waters, in permeable reactive barriers, and in filtration systems.

We used laboratory batch, column, and flow-through reactive cell experiments, chemical and structural analysis, and geochemical modeling to identify solution species and solid phases and to characterize the equilibria and character of the controlling reactions.

This research tests the hypothesis that in oxidizing hydroxyapatite-equilibrated waters, uranium is sorbed by inner-sphere complexation to phosphate and calcium oxide groups on the mineral surface. Data defining the relative extent of sorption as a function of pH, dissolved inorganic carbon, and ionic strength are necessary to understand the mechanisms of sorption.

Chapter Two is an overview of the aqueous chemistry of uranium and hydroxyapatite interaction with dissolved uranium, a review of previous work, and potential mechanisms for interaction between uranium and hydroxyapatite.

In Chapter Three, results are presented for proof-of-principal experiments to test the efficacy of the removal process and to define the equilibria, kinetics, and coordination of uranium on reacted hydroxyapatite.

Chapter Four presents the results of batch experiments with aqueous uranium and hydroxyapatite in: 1) ambient air, 2) a CO_2-free (argon) atmosphere, 3) a 0.5% CO_2 atmosphere, 4) a 1% CO_2 atmosphere, and 5) ambient air and a range of dissolved bicarbonate concentrations. Batch experiments were conducted by reacting hydroxyapatite with equilibrated buffer solutions and 0.1 to 10 ppb of dissolved uranium. We used equilibrium thermodynamic models to define equilibrium assemblages and mineral saturation indices for our experiments.

Chapter Five presents the results of two flow-through experiments. A first experiment was conducted with a reactive cell to load uranium onto a small mass of crystalline hydroxyapatite. This technique was used to determine the maximum loading of uranium per surface area of hydroxyapatite at near-neutral pH and ambient atmosphere. A second experiment comprised pumping uranium-bearing ground water through a column packed with cow bone char and sand. This column experiment simulated flow within a permeable reactive barrier for *in situ* removal of uranium from ground water.

2. Background

2.1. Aqueous Geochemistry of Uranium

Uranium occurs at average concentrations of 3 ppb in seawater; 0.1 to 500 ppb in surface waters, and 1 to 100 ppb in ground waters. In oxidized waters, U (VI) exists as the highly soluble uranyl ion ($UO2^{+2}$) and its complexes (Langmuir, 1978 and 1997; Meinrath et al., (1999). Uranium speciation in the absence of carbon is shown on Figure 2.1a. Carbonate complexes are the dominant uranyl species in most ground and surface waters (Murphy and Shock, 1999). At typical subsurface CO_2 partial pressures of about 10-2 atmospheres, the complexes $UO_2(CO_3)_2^{-2}$ and $UO_2(CO_3)_3^{-4}$ predominate above pH values of 6 and 7, respectively (Figure. 2.1b). Uranyl hydroxide complexes predominate at lower CO_2 partial pressures (Figure 2.1c). UO_2^{+2} is the dominant uranyl complex in solutions containing less than 10^{-4} to 10^{-3} M carbonate at acidic pH. U (IV) oxidation is enhanced by the carbonate and hydroxide complexes, which increase solubility and

provide electron donors. Fluoride, phosphate, and organic ligands may also form uranyl complexes. $UO_2(PO_4)^{-1}$ is the predominant uranyl phosphate phase in waters in equilibrium with uranyl phosphate minerals, such as calcium autunite ($Ca(UO_2)_2(PO_4)_2 \cdot 10H_20$). Uranium concentration in oxidized waters is controlled by a variety of hydroxide, carbonate, silicate, and phosphate minerals (discussed below).

Uranous ion, UO_2^0 [U (IV)], and its complexes predominate in ground waters of low Eh. Owing to the low solubilities of reduced solids (uraninite and pitchblende), U (IV) concentrations in reduced ground waters at low Eh are usually less than 10^{-8} M. (Langmuir, 1978).

In general, U (VI)) complexes are of inner-sphere character (Choppin, 1997). Exchange reactions between hydrated U (VI) and ligands are favored by the entropy increase caused by disruption of the hydration shell (Langmuir, 1978). U (VI) generally forms a six-fold coordination shell. The uranyl ion is linear with 1.82 angstroms between each of the two oxygen atoms and the central uranium atom (the two O_{ax} and the U in the center of Figure 2.2). In most complexes, this geometry is preserved, though interatomic distances change (Clark et al., 1995). X-ray techniques have successfully been used to determine the structure of uranyl carbonate (Allen et al. 1995), uranyl hydroxide (Meinrath, 1998), and uranyl oxide (Allen et al., 1996) surface and dissolved complexes.

The most important solubility-controlling phases for uranium in surface water and shallow-moderate depth ground water are schoepite ($UO_2(OH)_2{:}H_2O$), rutherfordine (UO_2CO_3), becquerelite ($Ca(UO_2)_6O_4(OH)_6 \cdot 8H_20$)), soddyite/weeksite ($Ca(H_2O)2(UO_2)_2$), and uranophane ($UO_2(SiO_2)_2(OH)_6$) (Langmuir, 1978 and 1997; Meinrath, 1997 and 1998; Murphy and Shock, 1999). Amorphous uranyl phases can also sequester uranium from solution. The least soluble of these minerals, schoepite, can control U (VI) concentrations to one to two ppm at typical surface conditions. In systems containing more than one ppm of phosphate, calcium autunite and hydrogen autunite may control aqueous uranium concentrations (Finch and Murakami, 1999). Such waters are not common, but are typical of the experiments conducted herein.

Sorption provides a means for fixing the uranium to the solid surface and can lead to mineralization. The pH range of minimum solubility of the uranyl minerals (generally near-neutral) is also that of maximum sorption. This is largely because the PNZC (point of net zero charge) for most mineral surfaces is at near-neutral pH. For example, Sylwester et al. (2000) used x-ray adsorption fine structure spectroscopy (XAFS) to determine that at near-neutral pH, uranyl sorbs to montmorillonite via inner-sphere, bidentate surface complexation.

In the presence of CO_2 (g), U (VI) sorption onto mineral surfaces is at a maximum at near-neutral pH (between 6.0 and 7.0), and decreases sharply toward more acidic or alkaline conditions (Sylwester et al., 2000). At low pH, U (VI) exists primarily as a mononuclear, aqueous ionic species, and outer sphere complexation is the primary mode of sorption (Kos, 1998). At about pH 5-6, de-protonation of surface hydroxyl groups provides additional sorption sites, and aqueous U (VI) hydroxyl species begin to form. These changes are accompanied by stronger inner-shell surface sorption and the formation of aqueous as well as sorbed polynuclear complexes, including surface precipitates. At still higher pH, in the presence of CO_2, U (VI) bicarbonate complexes dominate and retard sorption because in this pH range, mineral surfaces are

predominantly negatively charged. Sorption of U (VI) by organic matter may precede reduction to much less soluble U (IV) minerals.

2.2. Transport of Uranium in Ground Water Systems

There are three principal mechanisms of uranium immobilization in ground water systems: 1) precipitation of uranium-bearing solids, 2) sorption of dissolved U, and 3) filtration of colloidal uranium to mineral surfaces and/or organic matter.

Several factors control uranium transport. Changes in pH and Eh can result in changes in speciation and/or oxidation state that control the solubility of uranium-bearing minerals and thus the maximum dissolved concentration of uranium. Chelation with siderophore or complexation with inorganic species such as carbonate, hydroxide, and phosphate, are principal solubility controls that can lead to bioaccumulation, movement, or release due to dissolution of solid phases.

The extent and degree of uranium migration are determined by the rate and direction of ground water flow, the extent to which mineral assemblages of host rocks adsorb or release uranium, and changes in pH, dissolved oxygen and carbonate along the flow path that may cause dissolution or precipitation of uranium minerals.

Microbial processes may also have a profound effect on aqueous U. As a result of sluggish kinetics, redox reactions involving uranium can provide sources of metabolic energy for microbes (Suzuki and Banfield, 1999). Microbes can create enzymes that overcome the kinetic barriers to oxidize sulfide and ferrous iron and reduce U at the same time. The presence of other electron donors, such as sulfate, phosphate, and carbonate, can also hasten reduction of uranium to less soluble forms. Conversely, oxidation of uranium is accomplished by reduction of organic matter, iron, sulfur, or carbon (Langmuir, 1978). Bacteria often assist in the oxidation of uranium in ore. Living cell membranes are typically negatively charged and can sorb appreciable uranium, especially in low pH waters, where cationic forms of uranium predominate. Dead cells may also sorb uranium.

Besides existing as dissolved species, uranium can be transported in water as polymeric compounds of hydrolyzed U or sorbed and transported on natural colloids. Colloidal particles (10^{-5}-10^{-8} m diameter) include bacteria, clay particles, and large organic molecules. Where charged, colloids can interact and sorb to mineral surfaces. Colloidal uranium is typically not accounted for in thermodynamic speciation calculations and reactive transport models

2.3. Aqueous Chemistry of Uranium and Hydroxyapatite

Dissolved uranium in ground water interacts with hydroxyapatite ($Ca_5(PO_4)_3OH$) and its equilibrium dissolution products to remove uranium from solution by two processes: 1) formation of uranium phosphate solids such as the autunite minerals , and 2) sorption and ion exchange reactions at the mineral surface.

2.3.1. Uranyl Phosphate Mineral Equilibria

Valsami-Jones et al. (1998) studied hydroxyapatite dissolution from pH 2-7 and in the presence of dissolved metals. They determined that dissolution rate was sensitive to metals concentration and was slower when metals were present. Their work is important because they characterized surface complexes for lead and hydroxyapatite at variable pH.

At typical surface conditions, equilibrium of hydroxyapatite from undersaturation can take several days (Valsami-Jones et al., 1998). In the proper ratio of bicarbonate and phosphate, autunite can precipitate from solution (Sowder et al, 2000; Miyahara, 1993). At neutral pH, hydroxyapatite in equilibrium with water at concentrations in excess of 1 ppm or uranium can precipitate calcium autunite. The large K_{eq} for calcium autunite illustrates its ability to sequester uranium. The equilibria between dissolved uranium and relevant U (VI) minerals are depicted in Table 2.1. At uranium concentrations in excess of tens of ppb, these dissolution-precipitation reactions control the concentration of uranium in calcium phosphate-dominant waters, such as the solutions created for most of the experiments conducted in this research. In the absence of sufficient calcium and phosphate, hydrolysis products such as schoepite control uranyl solubility at ppm concentrations of uranium.

2.3.2 Sorption Reactions between Uranium and Hydroxyapatite

Workers have defined equilibria and mechanisms for sorption of many heavy metals (cadmium, chromium, lead, and zinc) to phosphate minerals (Chen et al., 1997a and 1997b). More recently, workers have conducted experiments involving uranium and phosphate minerals and the degree of uranium sequestration relative to pH and uranium concentration (Arey and Seaman, 1999; Admassu and Breese, 1999).

For solutions undersaturated with respect to calcium autunite (and other uranyl phosphate solids), uranium sorption to hydroxyapatite is the only mechanism for uranium removal. Hydroxyapatite possesses both phosphate and calcium oxide sites that can serve both as proton donors and proton receptors, depending on pH and major ion chemistry.

Below concentrations dictated by uranium mineral equilibria, aqueous uranium concentrations are controlled only by sorption and ion exchange reactions at mineral surfaces. Hydroxyapatite has a tetragonal structure and a particularly reactive mineral surface with an un-paired electron on each of 4 phosphate groups and 2 calcium oxide groups per unit cell. The structure and unit cell of hydroxyapatite are shown in Figure 2.3. Surface complexes bind by inner-sphere coordination to phosphate by mono- and bidentate complexation and calcium oxide by monodentate complexation. Ball-and-stick models depicting the likely coordination of aqueous uranyl to the hydroxyapatite surface are shown in Figure 2.2. In Section 3.5, we present results of x-ray absorption spectroscopy as used to identify the coordination of aqueous uranium to the hydroxyapatite surface.

Millard and Hedges (1996) found an increase in uranyl sorption to hydroxyapatite and bone material in the presence of carbonate. There is some contradiction in the literature about this. It appears that at lower carbonate concentrations, uranium may exist as $UO_2CO_3^0$ and $UO_2\ (CO_3)_2^{-2}$; these latter complexes may sorb more favorably than the more highly charged $UO_2(CO_3)_3^{-4}$ that will predominate at higher total carbonate concentrations. Thus above pH 7, as pH and carbonate increase, uranyl sorption to hydroxyapatite theoretically decreases.

Bostick et al. (2000) documented the effectiveness of hydroxyapatite and bone materials in removing uranium from synthetic ground waters. Fuller et al. (2002) performed batch experiments with hydroxyapatite at near-neutral pH and ppm-level uranium concentrations. They determined that for initial uranium concentrations, in excess of 99.5% of the uranium was removed by the hydroxyapatite. Fuller et al. (2002) used x-ray techniques to deduce that at up to 4700 ppm of uranium on hydroxyapatite, sorption is the primary mechanism for uranium removal. At uranium loadings on hydroxyapatite in excess of 7000 ppm, they found that chernikovite ($H_2(UO_2)_2(PO_4)_2 \cdot 10H_20$), also referred to as meta-autunite, had formed. At still higher uranium loadings, calcium autunite was detected.

Ordonez-Regil (2003) conducted sorption edge experiments with uranium on lanthanum phosphate. Their goal was to define specific thermodynamic data and reaction mechanisms. Lanthanum phosphate is much less soluble than hydroxyapatite and thus equilibrates at much lower aqueous concentrations of calcium and phosphate, than does hydroxyapatite. Thus, much higher concentrations of aqueous uranium can be used without uranium mineralization and thus uranium can be more completely loaded to the mineral surface during a batch experiment. They used an initial uranium concentration of 10^{-4} M (27 mg/L) and a solid liquid ratio of 10 mL to 0.1 g (0.1:1) and 0.2 g (0.1:2) of solid, respectively. They observed a drastic change in sorption percentage (from initial uranium) from pH 0.5 to 4.5 (30% at pH 1 to 95% at ph 4.5). As was expected there was a shift in the sorption edge to higher pH values at the higher solid:liquid ratio, presumably owing to the higher surface coverage. They also found reversibility (de-sorption to 50% of the initial U concentration after 24 h in a uranium-free KNO_3 bath) in a limited set of batch experiments. Ordonez-Regil et al. (2003) also determined the zeta potential and surface acidity constants for lanthanum phosphate. These data, together with the equilibrium distribution of U, enabled calculation of thermodynamic constants for U sorption to this mineral.

3. Proof-of-Principle Experiments

3.1. Introduction

We conducted batch experiments with crystalline hydroxyapatite, ceramic hydroxyapatite, fish bone, or cow bone char in ground water or a simple electrolyte solution containing dissolved uranium. These experiments were conducted to test the principle that hydroxyapatite removes uranium from solution and to define the steady-state uranium concentration and time to reach steady-state for different hydroxyapatite forms. Another goal was to create samples of reacted apatite and precipitates for x- ray absorption and diffraction analysis for comparison with known spectra of uranium surface complexes and minerals such as calcium autunite.

In preparation for this work, we calculated the theoretical maximum mass of uranium that can be sorbed to one m^2 of hydroxyapatite, or the sorption capacity, by defining the density of sorption sites on the hydroxyapatite surface or the number of phosphate and calcium oxide groups on a face of the unit cell. There are a total of three phosphate sites and one calcium site on the 0001 cleavage face (Figure 2.3). This face corresponds to the base of the unit cell of hydroxyapatite. The area of this face is 88.2 square-angstroms. Thus, one m^2 of crystalline hydroxyapatite contains 4.5×10^{18} potential sorption sites.

Assuming a 1:1 coordination of uranium to available sorption sites, 4.5 X 10^{18} atoms, 0.0000076 moles, or 18 mg of dissolved uranium would be necessary to fully saturate the sorption sites on one m^2 of hydroxyapatite. In Chapter 5, we compare this theoretical maximum calculation with results from reactive cell experiments.

3.1 Materials and Methods

The methods specific to this phase of the research are presented below. The methods also apply to experiments described later in this report. Methods specific to other phases of this research are described later in this report in the appropriate sections.

3.2.1. Materials

Four hydroxyapatite materials were used in this study. Fish bones were provided by PIMS NW, Inc. of Carlsbad, New Mexico. Prior to shipment, the fish bones were heated to over 300^o C to remove residue. Received fish bones were crushed and sieved to two size fractions. Cow bone char was provided by Brian Dwyer of Sandia National Laboratory and was used as received. The two types of pure hydroxyapatite used in this study were reagent-grade crystalline hydroxyapatite, manufactured by Sigma-Aldrich, Inc., and ceramic sintered amorphous hydroxyapatite manufactured by Bio-Rad, Inc. Mean grain diameter and surface area for these materials, as determined by sieving and the Brunauer-Emmett-Teller (BET) method, respectively, are listed on Table 3.1.

Owing to its purity and structure, the crystalline hydroxyapatite was used in the majority of the experiments described in this and later sections. This material yielded the x-ray diffraction (XRD) spectra of crystalline hydroxyapatite; the amplitude and width of the peaks (Figure 3.1) indicated crystal diameters generally in the 25 nm range. These "nanocrystals" within the larger hydroxyapatite crystal can be seen in the scanning electron microscope (SEM) image in Figure 3.2. The surface area measured for the hydroxyapatite (Table 3.1) can be accounted for as the surface area of a gram of hydroxyapatite comprised of 25 nm diameter spheres. Hydroxyapatite has a density of 3.2 g/cm^2. This calculation yields a surface area of 79.15 m^2/g. Thus, the surface area in Table 3.1 (82.2 m^2/g) appears reasonable. Furthermore, the surface area is not dependent on the size distribution of the larger clumps of "nanocrystals," and sieving is not necessary to separate hydroxyapatite of a constant surface area.

3.2.2. Methods

3.2.2.1. Experimental

For the majority of the proof-of-principle experiments, a 0.1 M $NaNO_3$ buffer solution was pre-equilibrated for at least 5 days with the hydroxyapatite of interest prior to the addition of uranium stock solution. After addition of uranium, the experimental bottles, typically 1 L in volume, were shaken at 22^o C for 5 days. Five days was found adequate for dissolution of the hydroxyapatite to steady-state as indicated by stabilizing electrical conductivity and aqueous calcium and phosphate concentrations. After pre-equilibration and immediately prior to beginning the experiment, all residual

hydroxyapatite was removed by centrifugation to prepare solutions for batch experiments. No attempt was made to control gas partial pressures and all initial solutions were allowed to equilibrate with the atmosphere.

Natural uranium-bearing ground water from LLNL Site 300 was also used in several of these experiments, but was not pre-equilibrated. These experiments were also conducted in 1L bottles.

Prior to use in experiments, all bottles were double-washed in nitric acid and triple-rinsed in de-ionized water. We added the required volume of uranium stock solution to yield the desired initial uranium concentration. Initial uranium concentrations were confirmed by analysis of 4 mL of 2% nitric acid spiked with equivalent volumes of stock solution. Typically, the hydroxyapatite was added to each bottle to create a 1:1000 solid:liquid ratio. The 1L bottles were placed in a temperature-controlled orbit shaker immediately after addition of the hydroxyapatite. Some experiments were also done at other solid:liquid ratios in 1L bottles. Still other experiments were conducted in 50 mL centrifuge tubes that were only used for one sample (for a single time step or solid:liquid ratio).

3.2.2.2. Analytical

A Hewlett-Packard Agilent HP4500 inductively-coupled mass spectrometer (ICP-MS) was used for analysis of dissolved uranium. Samples were collected through 0.2 micron polypropylene syringe filters or were centrifuged at 4500 rpm for 1 hour. Each 4 mL aliquot for uranium isotopic analysis was acidified with 1 M nitric acid to a pH below 2 and spiked with a thallium or uranium-238 standard. ICP-MS can analyze to exceedingly low uranium concentrations (< 10 pg/mL), and thus enable the determination of the equilibrium distribution of uranium from very low initial uranium concentrations of 0.01-10 ppb.

Measurements of pH were made with an Orion 250A or Micrometer Model 6072 pH meter and Orion 2100BN pH probe. For the initial experiments, pH meter calibration was performed with standard pH 4, 7, and 10 buffer solutions. Later calibrations were done using the Gran function titration method to correct for differences between measured hydrogen ion activity and actual hydrogen ion concentration that can occur when the ionic strength of calibration buffer solutions and the measured solution differ by orders-of-magnitude. A re-circulating water bath system was used to keep all titration vessels at a constant 22^{o} C temperature. Surface area was measured with a Micrometrics Gemini BET-1.0 surface area analyzer by the Brunauer-Emmet-Teller (BET) method. Each measurement was conducted in triplicate and the geometric mean was calculated as the result.

X-ray absorption spectroscopy was performed at the Stanford Linear Accelerator Center (SLAC) Synchrotron Source Radiation Laboratory (SSRL) on beam line 4-1 and spectra were analyzed by fitting to characteristic x-ray absorption curves to distinguish uranium-bearing coordination complexes and solids. FEFF software (University of Washington, 2002) was used to perform Fourier transform analysis and fit the measured curves to reference curves. A JEOL scanning electron microscope (SEM) was used for photomicrography. A Scintag Pad V x-ray diffractometer was used to collect x-ray diffraction spectra for determination of mineral composition and crystal diameters.

3.3. Results and Discussion

3.3.1. Batch Experiments with Natural Ground Water

Several initial experiments were conducted with uranium-bearing ground water collected from two monitoring wells (NC7-25 and NC7-40) at Lawrence Livermore National Laboratory Site 300, an explosives test facility in the Coast Range of Northern California. This ground water contained up to 500 mg/L of bicarbonate and about 8 ppm of dissolved oxygen (Taffet et al., 2004). Initial uranium concentrations were about 45 and 210-220 μg/L, respectively.

Figure 3.3 shows the change in dissolved uranium concentration with time for 30 mg of fine fish bone apatite reacted with 1 L of NC7-25 ground water. Initial uranium concentrations declined from 45 to 0.3 μg/L (a reduction of 99.33%) in less than 20 hours. The fish bone reduced dissolved uranium concentration to below the 30 μg/L MCL in less than 2 hours.

A comparison of the removal of dissolved uranium from NC7-25 ground water after 5 days of reaction with fine and coarse fish bone is shown on Figure 3.4 as a function of solid:liquid ratio by mass, and in Figure 3.5 as a function of surface area. It is apparent that the higher surface area per volume of solutions results in lower final dissolved uranium concentrations.

In preparation for designing a permeable reactive barrier field test for *in situ* removal of uranium in ground water at Site 300, we reacted four different masses of cow bone char with NC7-40 ground water containing an initial uranium concentration of 220.7 μg/L. Figure 3.6 shows the progress of the reaction between the cow bone char and ground water for the four solid:liquid ratios. The 0.4, 0.8, and 0.16 mg per 35 mL ground water experiments all reached steady-state within 10 hours. The partition coefficient, k_d, for the cow bone char was calculated as:

$$K_d = ((C_i - C_f)/m_{\text{cow bone char}})/C_f/V),$$ where:

C_i = initial uranium concentration,
C_f = final uranium concentration,
M = mass of cow bone char, and
V = volume of reacting ground water

The geometric mean of k_d from the four experiments was 1.99.

3.3.2. Batch Experiments with Several Forms of Hydroxyapatite and a Background Electrolyte

Figure 3.7 is a graph of the change with time from an initial uranium concentration of 10 ppb for pre-equilibrated 0.01 $NaNO_3$ in contact with two synthetic hydroxyapatite forms and coarse and fine fish bone. It is apparent that the crystalline and ceramic hydroxyapatites achieved steady-state uranium concentrations within just over 20 hours of reaction. These two types of hydroxyapatite reduced aqueous uranium concentrations to less than 0.03 μg/L within an hour. The two size fractions of fish bone may not have

reached steady-state at 120 hours; the fish bones reduced uranium concentrations less completely than the pure forms.

Figure 3.8 is a graph of dissolved uranium concentrations with time in 0.01 M $NaNO_3$ with an initial uranium concentration of 10 ppm in contact with the same four forms of hydroxyapatite as shown in Figure 3.7. The synthetic forms reduced aqueous uranium concentrations to below the uranium MCL (20 ng/mL) in less than 2 hours. Fish bones took over 60 hours to reach uranium MCLs and had not achieved steady-state concentrations by 120 hours.

3.3.3. Reversibility of Uranium Sequestration by Hydroxyapatite

Equilibrium isotherm batch experiments were conducted at initial uranium concentrations of 0.1 to 10 ppm and 0.1 to 100 ppb, respectively. At the conclusion of 5 days, the hydroxyapatite and the sorbed uranium were removed and reacted with uranium-free 0.1 M $NaNO_3$ for 5 days. Figure 3.9 shows the results of the first experiment. The graph shows that the reaction is reversible and that the equilibrium aqueous uranium concentrations were similar for the sorption and de-sorption reactions. Figure 3.10 shows the results of the 0.1 to 100 ppb initial uranium case. The reaction was also reversible in this range but differed from the higher concentration case in that the initial sorption of the uranium yielded 1-2 order of magnitude lower aqueous uranium concentrations than the de-sorption case. The cause of this counter-intuitive behavior will be studied in future experiments. The significance of the reversibility is two-fold. Reversibility implies that the sequestration of the uranium by hydroxyapatite is an equilibrium process. The reversibility also has implications for *in situ* treatment of uranium in ground water. If aqueous uranium concentrations decline, or sorptive capacity is reached, uranium can de-sorb from the solid. I*n situ* application would require regular monitoring of upgradient and downgradient uranium concentrations in ground to determine when the hydroxyapatite might leach uranium to ground water.

3.3.4 Isotherm Batch Experiment at pH 4 and 7

Equilibrium batch experiments were conducted at initial uranium concentrations of 0.01 to 10 ppb at pH 4 and pH 7 for 5 days. Figure 3.11 shows the sorption isotherms. The isotherms are similar for pH 4 and pH 7. The steady-state aqueous uranium concentrations are generally higher for the pH 7 case, which exhibits Langmuir isotherm behavior.

A series of batch experiments were also conducted at pH 7 in which changes in a range of initial uranium concentrations were compared for 0.01M $NaNO_3$ solutions where hydroxyapatite was present and in which it was removed after pre-equilibration. The purpose of the experiments was to deduce the threshold aqueous uranium concentration for precipitation of uranium phosphate solids. Dissolved uranium concentrations did not decline in equilibrated solutions without hydroxyapatite containing less than 20-50 ppb, but did decline in equivalent solutions containing hydroxyapatite. Thus, sorption appears to control uranium removal below 20-50 ppb of uranium in apatite-equilibrated solutions containing hydroxyapatite. Uranium phosphate solids can form in hydroxyapatite-equilibrated solutions containing in excess of 20 ppb uranium.

3.3.5. Ionic Strength Batch Experiments

Equilibrium batch experiments were conducted at ionic strengths (I) of 0.005 to 0.1 and initial uranium concentrations of 0.14 and 6 ppb. The results indicate an extremely small but measurable effect of ionic strength on sorption (Figure 3.12). This effect is more pronounced for the 6 ppb case. For instance, at I = 0.01, sorption reduced aqueous uranium concentration by 99.97%. At I = 0.1, sorption reduced uranium concentration by 99.90%. This difference is insignificant in terms of its effect on equilibrium sorption.

3.3.6. Characterization of Reacted Hydroxyapatite Materials

To identify, coordination of uranium to the mineral surface and to discern any solid uranium phosphate phases, samples of fish bone and crystal and ceramic apatite from the previous experiments were analyzed by extended x-ray absorption fine structure (EXAFS) near-edge and L_{III} absorption edge techniques. We used EXAFS to investigate oxidation state and coordination of sorbed U. Near-edge data indicate that uranium on crystalline apatite remains in the U (VI) oxidation state, so sorption does not involve a redox process. Figure 3.13 depicts Fourier transforms of the U L_{III} absorption edge data for three hydroxyapatite forms from batch experiments (aqueous uranium concentration of 8.3 ppm). The U L_{III} absorption edge corresponds to the photon energy at which there is just enough energy to eject a 2p 3/2 electron from the uranium atom. At this energy, the plot of absorption intensity versus energy contains a step jump-called an "edge." These data show uranium ions (UO_2^{2+}) bound to phosphate as a surface complex, and possible uranyl phosphate precipitates. All samples showed similar fits with bidentate sorption to calcium and monodentate (coordinated to one oxygen molecule) and bidentate (coordinated to two oxygen molecules) sorption to phosphorus.

To investigate the competing processes of autunite precipitation and surface complexation on the apatite surface, samples with high and low concentrations of uranium were prepared. The high-concentration sample (17 wt% uranium) has nearly identical EXAFS spectra to a reference autunite. The low-concentration samples (4% uranium by weight) were prepared by batch reactor addition of uranium onto crystalline apatite for 4 weeks while maintaining solution uranium concentrations at less than 10 ppb. The EXAFS data indicate that up to several thousand parts U per million parts hydroxyapatite, surface complexation, and not precipitation, is the predominant process.

3.2 Summary and Conclusions

Our experiments indicated that crystalline and ceramic hydroxyapatite and fish bone apatite reduced aqueous uranium concentrations. The crystalline and ceramic forms reduced uranium concentrations faster due to their larger surface areas and greater percentage of hydroxyapatite. With sufficient time and solid:liquid ratio, all forms of hydroxyapatite could reduce aqueous uranium to below drinking water MCLs (30 ppb).

The reactions between aqueous uranium and hydroxyapatite are reversible, which indicates that sorption and precipitation are likely equilibrium processes. The reversibility of these reactions has implications for in situ ground water treatment.

Ionic strength has little effect on sorption equilibria.

Sorption is the only process for uranium removal in solutions in contact with hydroxyapatite at uranium concentrations below 20-50 ppb. Mineralization of uranium phosphate may occur in hydroxyapatite-equilibrated solutions at aqueous uranium concentrations in excess of 20 ppb.

EXAFS data show uranium bound to phosphate as a surface complex, and possible uranyl phosphate precipitates. All samples showed similar fits with bidentate coordination to calcium oxide and monodentate and bidentate coordination to phosphate. The high concentration sample (17 wt% uranium to weight of hydroxyapatite) has nearly identical EXAFS spectra to a reference autunite. The low concentration samples (4% uranium by weight) only indicated surface complexation. The EXAFS data indicate that up to several thousand parts uranium per million parts apatite, surface complexation is the predominant process.

4. Sorption Experiments in Ambient and CO_2-controlled Atmospheres

4.1. Introduction

Experiments that define the dependence of solute sequestration on pH are often referred to as sorption edge experiments (Langmuir, 1997). This section details the results of batch experiments conducted at pH range 4-10 in hydroxyapatite-equilibrated 0.01 M $NaNO_3$ in equilibrium with air at several CO_2 concentrations: atmospheric (0.03%) and 0%, 0.5%, and 1%. The principal purpose of these experiments was to define the effects of pH and dissolved inorganic carbon on steady-state sorption of uranium on hydroxyapatite at initial uranium concentrations of 0.1 to 10 ppb. This understanding would elucidate the potential limitations of pH and dissolved inorganic carbon on sorption in uranium-contaminated waters and the sorptive behavior of uranium in phosphate-bearing aquifers and the mineral deposits arising from them. We used geochemical modeling to determine the speciation of uranium in solution and saturation indices of uranium, carbonate, and phosphate minerals in experimental solutions. Effects of ionic strength on sorption were also evaluated, because this equilibration process resulted in higher ionic strengths in solutions at low and high pH (4-5 and 9-10).

4.2 Materials and Methods

4.2.1 Materials

We used reagent-grade crystalline hydroxyapatite in these experiments. This hydroxyapatite was used to pre-equilibrate background electrolyte solutions and as the sorbent in the batch experiments.

4.2.2. Methods

4.2.2.1. Experimental

Background electrolyte solutions were pre-equilibrated with crystalline hydroxyapatite for at least five days to minimize mineral dissolution as a variable that could affect the sorption process. At least 0.2 g of apatite were added to each L of $NaNO_3$ in Milli-Q water. To maintain a consistent ionic strength of approximately 0.2 M across the pH range, $NaNO_3$ buffer solutions were prepared at specific concentrations for each of the seven steps (from pH 4-10). Pre-equilibrated solutions were prepared and shaken for 5 days. We adjusted the pH of each solution to the nearest whole digit, i.e., pH 4.0, etc. by adding small volumes of 0.1 M NaOH or 0.1 M HCl, measuring pH, and continuing shaking until pH had stabilized to within 0.05 units. After adjustment, solutions were sealed with film to minimize further interaction with the atmosphere and were used in experiments within a week.

A glovebox was used to prepare pH-specific hydroxyapatite equilibrated solutions and to run experiments. Argon gas was used for the CO_2-free case. CO_2 gas was supplied at 0.5% and 1%. Gas cylinders were connected to the glovebox and air was evacuated until equivalent CO_2 gas concentrations existed in the gas cylinder and the glovebox. Solution pH was also adjusted in the glovebox. Upon addition of ^{233}U, a circular shaker was used to shake the experimental solutions. No attempt was made to control gas partial pressures for the atmospheric case and all initial solutions were allowed to equilibrate with the atmosphere. Before beginning each experiment, 50 mL tubes of each pH-and hydroxyapatite-equilibrated solution was centrifuged for 10 minutes at 4500 rpm to yield 35 mL of solution for each batch experiment.

A group of 7 samples (one for each pH step from approximately 4-10), was created for each initial U concentration. We added 0.035 g of apatite to each tube, shook the tubes, and added the required volume of ^{233}U stock solution to yield target ^{233}U concentrations of 0.1, 1.0, and 10.0 ppb. ^{233}U stock solution was used to enable discrimination of final U concentrations from background uranium to several ng/mL (ppt). ^{233}U has since been used as the uranium stock in all experiments with artificial buffer solutions. Initial ^{233}U concentrations were confirmed by analysis of 35 mL of 2% nitric acid spiked with equivalent volumes of ^{233}U stock solution to assure that the added uranium was not affected by inaccurate stock addition, hydrolysis, or sorption to the container walls.

Prior to beginning each batch experiment, samples were collected from each pre-equilibrated stock solution for major ions and total inorganic carbon. At the conclusion, we again collected samples of supernatant for analysis of these parameters and ^{233}U. The reacted hydroxyapatite and tube from each batch experiment were saved for later characterization and determination of mass conservation.

We ran a fifth round of batch experiments at bicarbonate alkalinities of 10 to about 900 mg/L. The same procedures were used to run these experiments as the atmospheric CO_2 case. To create solutions of varying bicarbonate alkalinity, reagent grade sodium bicarbonate was mixed with sodium nitrate to yield a constant ionic strength of about 0.02.

4.2.2.2.Analytical

Analytical methods for uranium were the same as previously described in Section 3.2.2.2. Activation Laboratories in Ancaster, Ontario, Canada (Actlabs-Ancaster)

performed major and minor ion analyses. They analyzed metals by ICP-MS or ICP-OES (optical emission spectroscopy). Anions were quantified by ion chromatography. Some of the major ion analyses were performed at LLNL by ion chromatography.

The vast majority of dissolved inorganic carbon concentrations were determined with an OI Corporation infrared gas analyzer 3300524D (CO_2 @ 0-400 ppm) after adding phosphoric acid to the water and off-gassing all carbon as CO_2 within an OI Corporation Ampule 524D analyzer unit. When not measured as converted CO_2, dissolved inorganic carbon was measured by alkalinity titration. Phosphate was analyzed by the phosphomolybdate method using a Varian Cary 500 Scan UV-VIS-NIR Spectrophotometer to measure the absorbance of the samples at 880 nm.

Measurements of pH were made as previously described in Section 3.3.2.2. For the initial experiments, calibration was performed with standard pH 4, 7, and 10 buffer solutions. Later work was conducted by calibration using the Gran function titration method to correct for differences between measured hydrogen ion activity and actual hydrogen ion concentration that could occur across ionic strengths spanning several orders of magnitude or by using pH buffers of different ionic strength from my experimental solutions. All titration vessels were kept at a constant 22^o C temperature with a Lauda-Brinkmann Model 301 re-circulating water bath system and were magnetically stirred while adding acid and taking manual readings of eV.

4.2.2.3.Data Analysis Methods

Initial and final major-ion and uranium analytical results and pH for each experiment were entered into the geochemical equilibrium speciation model REACT (Geochemist's Workbench, Bethke, 2000) to enable determination of the distribution of uranium-bearing species and relevant mineral equilibria. For the experiments conducted outside the glovebox, dissolved oxygen concentrations were not measured but were assumed to be in equilibrium with the atmosphere (8.38 mg/L dissolved oxygen at 22 deg C). Equilibrium speciation modeling was initially performed as a planning tool to define the possible threshold (concentration distribution of calcium, inorganic carbon/dissolved CO_2, phosphate, uranium, ionic strength, and pH) for the uranium-bearing minerals most likely to precipitate at the chemical conditions of interest (calcium autunite, hydrogen autunite, rutherfordine, becquerellite, and schoepite). Prior to beginning the modeling, we assembled an internally-consistent thermodynamic database from the NEA (Grenthe et al., 1992) and Langmuir (Langmuir, 1997) thermodynamic databases. I simulated the equilibrium chemistry of waters at variable pH and dissolved CO_2 in the presence of hydroxyapatite and calcium- and meta- (hydrogen) autunite (autunite and chernikovite, respectively) to determine the solubility of hydroxyapatite and autunite and to define the anticipated/theoretical distribution of dissolved uranium, calcium, and phosphate and the speciation of uranium.

4.2.3. Results and Discussion

Figure 4.1 is a summary of the results of steady-state uranium concentration and final pH for the four different air percent CO_2 cases at initial uranium concentrations of approximately 0.1, 1.0, and 10 ppb. The data generally show that uranium sorption is

strongest in the absence of CO_2 and weakest at 1% air CO_2, i.e., that the greater the percent CO_2 in air in equilibrium with the experimental solutions, the less strongly sorbed uranium is to hydroxyapatite. These data show little variability in solution equilibrium uranium concentration with pH. At pH 4 and pH 10, sorption was generally slightly weaker than at intermediate pH. Figure 4.2 is a plot of the percent of initial aqueous uranium concentrations removed for each of the four air CO_2 cases at each pH. Except for a few notable exceptions, uranium removal exceeded 97% and typically exceeded 98-99%. The notable exceptions were the 1% air CO_2 cases. The 1% air CO_2 cases at pH 9-10, yielded aqueous uranium reductions as low as 35-45%.

Figures 4.1 and 4.2 show that waters in equilibrium with the range of CO_2 concentrations characteristic of surface and subsurface waters, hydroxyapatite can remove the vast majority of uranium (over 95% of the uranium) in all but the highest pH cases with 1% CO_2 atmosphere. The range of bicarbonate alkalinities measured in the solutions ranged from 0 ppm (all pH steps) for the 0% air CO_2 case, 1.15 ppm (pH 4) to 25 ppm (pH 10) for the atmospheric case, 0.14 ppm (pH 4) to 200 ppm (pH 10) for the 0.5% air CO_2 case, and 0.42 ppm (pH4) to 390 ppm (pH 10) for the 1% air CO_2 case. For clarity, Figures 4.3, 4.4, and 4.5 depict the steady-state concentrations of uranium for the pH 4 to pH 10 cases previously summarized in Figure 4.1. In the next section, we discuss the results of uranium sorption for bicarbonate alkalinities of 10 to 900 ppm at near-neutral pH.

To determine the effects that uranium speciation might have on sorption, we modeled aqueous speciation with the program REACT. The program also provided saturation indices for minerals in each solution, which allowed confirmation as to whether, based on thermodynamic calculations, the solutions were close to saturation with hydroxyapatite and below saturation with uranium minerals.

Molalities of aqueous uranium species and saturation indices for relevant minerals for the 10 ppb initial uranium experiments for each of the atmospheric and 0% and 1% air CO_2 scenarios are shown in Figures 4.6 through 4.10. The 0.1 and 1.0 ppb initial aqueous uranium cases are not presented here but show similar dominant uranium species at each pH step and similar mineral saturation indices.

Figure 4.6 and Figure 4.7 show uranium speciation and mineral saturation indices, respectively for the atmospheric CO_2 case and 10 ppb initial uranium. $UO_2HPO_{4\ (aq)}$ is the dominant uranium species at low pH. $UO_2PO_4^{-1}$ dominates at moderate pH. $UO_2(CO_3)_3^{-3}$ dominates at high pH. No uranium minerals were saturated or supersaturated in any experimental solutions.

Figure 4.8 and Figure 4.9 show uranium speciation and mineral saturation, respectively for the 0% air CO_2 case and 10 ppb initial uranium. Again, $UO_2HPO_{4\ (aq)}$ is the dominant uranium species at low pH and $UO_2PO_4^{-1}$ dominates at moderate pH. However, due to the lack of carbon, $UO_2(OH)_3^{-1}$ predominates at high pH. Uranium minerals were not saturated or supersaturated in any experimental solutions.

Figure 4.10 and Figure 4.11 show uranium speciation and mineral saturation, respectively for the 1.0% air CO_2 case and 10 ppb initial uranium. Again, $UO_2HPO_{4\ (aq)}$ is the dominant uranium species at low pH and $UO_2PO_4^{-1}$ dominates at moderate pH. $UO_2(CO_3)_2^{-2}$, and then $UO_2(CO_3)_3^{-3}$, dominate at progressively higher pH. Uranium minerals were not saturated or supersaturated in any experimental solutions.

Figure 4.12 shows the distribution of steady-state aqueous uranium concentrations with pH for a range of bicarbonate alkalinities of 10-900 ppm. Figure 4.12 shows that uranium removal is greatest at bicarbonate alkalinities of 100-200 ppm and is least at alkalinities in excess of 800 ppm. It is noteworthy that the curves are all U-shaped.

Molalities of aqueous uranium species and saturation indices for relevant minerals for the 10 ppb initial uranium case across the range of bicarbonate alkalinities are shown in Figures 4.13. Figure 4.14 shows the mineral saturation indices for these experiments. $UO_2(CO_3)_2^{-2}$ and $UO_2(OH)_3^{-1}$ predominate at pH 4. $UO_2(CO_3)_3^{-3}$ dominates at all higher pH values. Uranium minerals were not saturated or supersaturated in any experimental solutions.

Sorption edges (pH range where U sequestration percentage changes dramatically) were not apparent for any of these experiments. The lack of a true sorption edge is typical of many dissolved metals at trace concentrations in water in contact with a surface reactive mineral such as iron oxide or hydroxide and clay (Langmuir, 1997). The important point to remember is that with few exceptions, regardless of air CO_2 concentration and pH, sequestration is very complete.

Equilibrium thermodynamic modeling of the solution chemistries indicates that for all three initial U concentrations and all air CO_2 and bicarbonate alkalinity cases, uranium species in the water are predominantly neutrally-charged at low pH and negatively-charged at moderate-to-high pH values. Determination of the point of non-zero charge (PZNC) would aid in the determination of the effects of surface charge on sorption. However, none are apparent at these low U loadings. Langmuir (1997) presents a PZNC of less than or equal to 8.5 for hydroxyapatite. Assuming that the PZNC of hydroxyaptite is somewhere between 7 and 8.5, predominantly negatively-charged uranyl species would be sorbing to a predominantly negatively charged surface above pH 7, and predominantly neutrally-charged uranyl species would be sorbing to a predominantly positively-charged surface below pH 6.5. Thus, sorption is either not significantly influenced by charge or at these trace concentrations of aqueous uranium there are still sufficient sites of opposite charge to promote for sorption.

It is clear that regardless of the mechanism responsible, uranium is generally almost completely removed from solution (in excess of 97%) for these chemical conditions, which reflect the typical aqueous chemistries that may be encountered in surface and subsurface waters.

4.2.4. Summary and Conclusions

The preceding experiments indicate that sorption of uranium to hydroxyapatite is very strong (in excess of 97% uranium concentration reduction) for all typical surface and subsurface conditions of bicarbonate alkalinity and pH, except for systems where pH exceeds 9 and bicarbonate alkalinity exceeds 100-200 ppm. In such high pH systems, sorption may not be as effective. Other than the reduction in sorption equilibria observed above pH 9 for the 1% air CO_2 case, there is no pH range where sorption equilibria change markedly.

Our results also indicate that in solutions with very low concentrations of uranium (0.1 to 10 ppb aqueous uranium), sorption may not be controlled by charge The preponderance of uranium that exists as neutrally-charged species at low pH suggests and

the high uranium removal under these conditions suggest that surface complexation of uranium on hydroxyapatite is not electrostatic.

5. Column and Flow-through Experiments

5.1 Introduction

Several flow-through experiments were performed to determine the sorptive capacity of hydroxyapatite. In this section we describe the results of a reactive cell experiment with crystalline hydroxyapatite and a column experiment with cow bone char and LLNL Site 300 ground water.

5.2 Methods

5.2.1. Materials

Reagent-grade crystalline hydroxyapatite, manufactured by Sigma-Aldrich, Inc., was used in the stirred cell experiment. Cow bone char, provided by Brian Dwyer of Sandia National Laboratory, was used as received.

5.2.2. Experimental

5.2.2.1. Reactive Cell Experiment

The reactive cell experiment was run by pumping (at 0.15 mL/min with a peristaltic pump) a 0.01 M $NaNO_3$ solution containing 1 ppm of aqueous uranium (1 ppm of natural uranium and 3 ppb of ^{233}U) into a 45 mL polypropylene cell. The cell was continuous stirred with a magnetic stirrer and contained an initial 20 mg of crystalline hydroxyapatite. Tritium was added to the initial uranium solution to enable determination of breakthrough (the time when pumped solution completely replaced the initial pre-uranium solution). Effluent samples were collected by an automated fraction collector. Uranium mass in solutions was measured by ICP-MS, as described previously. Calcium and phosphate concentrations were measured by liquid ion chromatography. Bicarbonate alkalinity was also measured as described previously. The experiment was run to the point where uranium concentrations reached their initial levels. The experiment was then continued by replacing the influent solution with uranium-free 0.01 $NaNO_3$ solution until uranium was de-sorbed from the hydroxyapatite to a point where a new equilibrium was established. Once the experiment was completed, the hydroxyapatite was removed and was subjected to XRD analysis.

5.2.2.2. Bone Char Column Experiment

A 1.5 cm diameter and 10 cm long borosilicate glass column was filled with a 50:50 (by volume) mixture of cow bone char and clean quartz sand. The volume of the column was 12.18 mL. The volume of pores was about 7.12 mL. The mass of bone char in the column was about 0.47 g, which equates to 19.93 m^2 of surface area. The column was

connected to a peristaltic pump and two pore volumes of de-ionized water was pumped upward through the column prior to pumping of water from Site 300 well NC7-40. The ground water contained about 260 ppb of uranium and was pumped upward through the column at an initial flow rate of 0.0089 mL/min with a standard deviation of 2.17%. Tritium was added to the initial uranium solution to enable determination of breakthrough (the time when pumped solution completely replaced the initial pre-uranium solution). Effluent samples were collected by an automated fraction collector. Uranium mass in solutions was measured by ICP-MS, as described previously. Calcium and phosphate concentrations were measured by liquid ion chromatography. Bicarbonate alkalinity was also measured as described previously. The experiment was run until and beyond breakthrough of uranium (about 950 pore volumes).

5.2.3. Results and Discussion

5.2.3.1. Reactive Cell

Figure 5.1 shows the progress of the reactive cell experiment. About 11,581.7 mL of uranium-bearing solution were pumped through the reactive cell before the influent uranium concentration was reached ($C/C_0 = 1$) within the cell and effluent. The uranium-bearing influent solution was not pre-equilibrated with hydroxyapatite to enable use of higher influent uranium concentrations while avoiding formation of uranium phosphate precipitates. An influent uranium concentration of 1 ppm was used because lower influent uranium concentrations would have resulted in complete hydroxyapatite dissolution prior to achievement of steady-state. In fact, 9.4 mg of the original 20 mg of hydroxyapatite were dissolved by the point where $C/C_o = 1$ was reached. The reaction resulted in the sequestration of 6.22 mg of aqueous uranium on 10.6 mg of hydroxyapatite. This equates to about 2.99×10^{-5} moles or 7.14 mg of sequestered uranium per m^2 of hydroxyapatite. Previous calculations described in Section 3.1, based on the density of sorption sites on the hydroxyapatite surface estimated from the unit cell, yielded a sorption capacity of 7.53×10^{-6} moles or 1.8 mg of uranium per m^2 of hydroxyapatite. The excess uranium removed in the experiment may be due to precipitation of uranium solids.

XRD analysis of the reacted hydroxyapatite indicated that meta-autunite was present (Figure 5.3). The reacted hydroxyapatite contained 27% uranium by weight. This confirms what was observed in EXAFS analysis of samples in Section 3.36, where fish bone containing 17% sequestered uranium also contained meta-autunite.

5.2.3.2. Bone Char Column Experiment

Figures 5.3 and 5.4 depict the results of the cow bone char column experiment. The initial flow rate was about 0.089 mL/min. The influent uranium concentration was about 260 ppb. Effluent uranium concentration dropped by over 80% at one pore (column) volume and reached a steady-state concentration of 0.3 to 0.4 ppb by about 65 pore volumes. The uranium MCL was reached in 1.5 pore volumes. Effluent uranium concentrations began rising at about 366 pore volumes and the flow rate was increased 10-fold to about 0.89 mL/min, whereupon effluent uranium concentrations rose quickly.

The experiment was stopped at 932 pore volumes when the effluent contained 46.5 ppb of uranium. At cessation of the experiment, the cow bone char had accumulated 1.67 mg of uranium, which equated to 3.52 X 10^{-7} moles or 0.083 mg of uranium per initial m^2 of cow bone char. This is one order-of-magnitude less than the calculated mass of uranium that can theoretically be removed by one m^2 of pure crystalline hydroxyapatite. The reacted cow bone char contained 3.5% uranium by mass. The initial cow bone char mass was 0.47 g. Assuming that no phosphorus-bearing solids were formed in the column during the experiment, about 50 mg of cow bone hydroxyapatite were dissolved, yielding a final cow bone char mass of 0.42 g. In this case, the cow bone char would contain 4.0% uranium by mass.

The reaction between the cow bone and NC7-40 ground water resulted in steady-state effluent phosphate concentrations of about 0.2 ppm. At steady state, effluent calcium concentrations were about 90% of the influent ground water concentrations, suggesting that a calcium-bearing solid was precipitating in the column. The pH stabilized at about 8.5. Chemical modeling will be conducted to calculate saturation indices and equilibria for the column chemical data.

5.2.4. Summary and Conclusions

Column and flow-through experiments indicated different capacities for sequestration of uranium in a simple electrolyte solution by pure crystalline hydroxyapatite and removal of uranium from ground water by cow bone char. The first case is an idealized scenario with pure mineral and a simple solution, while the second reflects a realistic scenario to which hydroxyapatite remediation might be applied. The crystalline hydroxyapatite sequestered appreciably more uranium as a function of surface area and mass. Crystalline hydroxyapatite sequestered 2.9 mg of uranium per m^2 as opposed to 0.083 mg of uranium sequestered per m^2 of cow bone char, or 27% versus 3.5% by surface area, respectively.

Aqueous concentrations of calcium and phosphorus and pH were not appreciable affected by cow bone char dissolution during the column experiment. Thus, it appears that emplacement of cow bone char within an aquifer for in situ remediation will not create adverse chemical conditions.

Despite its ability to lower aqueous uranium concentrations to below MCLs, the sorptive capacity of cow bone char may be limited. Other hydroxyapatite-bearing media may be preferable for treatment of uranium-bearing ground water. The use of higher solid:liquid ratios may make the cow bone char more effective.

6. Summary and Conclusions

Our experiments indicated that crystalline and ceramic hydroxyapatite and fish bone apatite reduced aqueous uranium concentrations. The crystalline and ceramic forms reduced uranium concentrations faster due to their larger surface areas and greater percentage of hydroxyapatite. With sufficient time and solid:liquid ratio, all forms of hydroxyapatite could reduce aqueous uranium to below drinking water MCLs (30 ppb).

The reactions between aqueous uranium and hydroxyapatite are reversible, which indicates that sorption and precipitation are likely equilibrium processes. The

reversibility of these reactions has implications for *in situ* ground water treatment. Monitoring of upgradient and downgradient ground water chemistry will be critical to defining when the hydroxyapatite treatment media would require replacement to avoid de-sorption of uranium to ground water.

Ionic strength has little effect on sorption equilibria. This finding is important, because it means that even brackish waters can be treated with hydroxyapatite to remove uranium.

Sorption is the only process for uranium removal in solutions in contact with hydroxyapatite at uranium concentrations below 20-50 ppb. Mineralization of uranium phosphate may occur in hydroxyapatite-equilibrated solutions at aqueous uranium concentrations in excess of 20 ppb.

EXAFS data show uranium bound to phosphate as a surface complex, and possible uranyl phosphate precipitates. All samples showed similar fits with bidentate coordination to calcium oxide and monodentate and bidentate coordination to phosphate. A high uranium concentration hydroxyapatite (17 wt% uranium to weight of hydroxyapatite) had nearly identical EXAFS spectra to a reference autunite. The low concentration hydroxyapatite (4% uranium by weight) only indicated surface sorption. EXAFS data indicate that up to several thousand parts uranium per million parts apatite, surface complexation is the predominant process. At higher concentrations of uranium on hydroxyapatite, meta-autunite precipitates. This finding is important because a given mass of hydroxyapatite can sequester a greater mass of uranium from solution by precipitation than from sorption.

The experiments described previously indicate that sorption of uranium to hydroxyapatite is very strong (in excess of 97% uranium concentration reduction) for all typical surface and subsurface conditions of bicarbonate alkalinity and pH, except for systems where pH exceeds 9 and bicarbonate alkalinity exceeds 100-200 ppm. In such high pH systems, sorption may not be as effective. Other than the reduction in sorption equilibria observed above pH 9 for the 1% air CO_2 case, there is no pH range where sorption equilibria change markedly.

As bicarbonate alkalinity increases above 500 ppm, there is a small but measurable reduction in uranium sorption to hydroxyapatite. In all cases from 10 to 900 ppm bicarbonate, uranium sorption percentage was always in excess of 98% at near-neutral pH.

Our results also indicate that in solutions with very low concentrations of uranium (0.1 to 10 ppb aqueous uranium), sorption may not be controlled by charge The preponderance of uranium that exists as neutrally-charged species at low pH suggests and the high uranium removal under these conditions suggest that surface complexation of uranium on hydroxyapatite is not electrostatic.

Column and flow-through experiments indicated different capacities for sequestration of uranium in a simple electrolyte solution by pure crystalline hydroxyapatite and removal of uranium from ground water by cow bone char. Crystalline hydroxyapatite sequestered appreciably more uranium as a function of surface area and mass than did cow bone char. Crystalline hydroxyapatite sequestered 2.9 mg of uranium per m^2 as opposed to 0.083 mg of uranium sequestered per m^2 of cow bone char, or 27% versus 3.5% by surface area, respectively.

Aqueous concentrations of calcium and phosphorus and pH were not appreciably affected by cow bone char dissolution during the column experiment. Thus, it appears that emplacement of cow bone char within an aquifer for *in situ* remediation will not create adverse chemical conditions.

Despite its ability to lower aqueous uranium concentrations to below MCLs, the sorptive capacity of cow bone char may be limited. Other hydroxyapatite-bearing media may be preferable for treatment of uranium-bearing ground water. The use of higher solid:liquid ratios may make the cow bone char more effective.

Additional data analysis and geochemical modeling are underway and should elicit additional insight into the experimental results presented here. These results will be presented in future publications.

7. Acknowledgments

The author and technical contributors would like to thank the following people for their assistance with this project: Ross Williams, Max Hu, Scott Szechenyi, Leslie Ferry, Fred Hoffman, Albert Lamarre, Judy Steenhoven, Dorothy Bishop, Sue Martin, Christina Ramon, Bill Casey, Mark Grismer, Brian Dwyer, Jim Conca, Judith Wright, Kevin Knauss, Roald Leif, Kim Heyward, Rosanne Depue, Linda Cohan, and Ken Moody.

8. References

Abdelouas, A., L. Lutze, and H.E. Nuthall (1999) Uranium contamination in the subsurface: characterization and remediation in: Uranium: Mineralogy, Geochemistry, and the Environment, Reviews in Mineralogy, V. 38, Mineralogical Society of America, Washington DC, Burns and Finch eds, pp. 422-474.

Admassu, W. and T. Breese (1999) Feasibility of using natural fishbone apatite as a substitute for hydroxyapatite in remediating aqueous heavy metals, Journal of Hazardous Materials 69(2): 187-196.

Allen, P.G., D.K. Shuh, J.J. Bucher, N.M. Edelstein, C.E.A. Palmer, R.J. Silva, S.N. Nguyen, L.N. Marquez, and E.A. Hudson (1996) Determinations of uranium structures by EXAFS: schoepite and other U(VI) oxide precipitates, Radiochimica ACTA, v.75, pp. 47-53.

Allen P.G., J.J. Bucher, D.L. Clark, N.M. Edelstein, S.A. Ekberg, J.W. Gohdes, and E.A. Hudson (1995) Multinuclear NMR, Raman, EXAFS, and x-ray diffraction studies of uranyl carbonate complexes in near-neutral aqueous solution, Inorganic Chemistry, v.34, n.19, pp.4797-4807.

Arey, J. S., J. C. Seaman, et al. (1999) Immobilization of uranium in contaminated sediments by hydroxyapatite addition. Environmental Science & Technology 33(2): 337-342.

Bethke, C.M. (2000) The Geochemist's Workbench: A Users Guide to RXN, ACT2, TACT, REACT, GTPLT, and Xt, University of Illinois, Champaign-Urbana, IL and Rockware, Inc, Laramie, WY.

Bostick, W., R. Stevenson, R. Jarabek, and J. Conca (2000) Use of apatite and bone char for the removal of soluble radionuclides in authentic and simulated DOE groundwater, Advances in Environmental Research, v.3, no. 4, pp. 488-498.

Burns, P.C. and R. Finch (1999) Uranium: Mineralogy, Geochemistry, and the Environment, Reviews in Mineralogy, V. 38, Mineralogical Society of America, Washington DC, 679 pp.

Chen, X. B., J. V. Wright, and J. Conca (1997a) Evaluation of heavy metal remediation using mineral apatite, Water Air and Soil Pollution 98(1-2): 57-78.

Chen, X. B., J. V. Wright, and J. Conca (1997b) Effects of pH on heavy metal sorption on mineral apatite, Environmental Science & Technology 31(3): 624-631.

Choppin, G.R. (1997) Inner versus outer sphere complexation of f-elements, Journal of Alloys and Compounds, v.249, pp. 9-13.

Clark, D.L., D.E. Hobart, and M.P. Neu (1995) Actinide carbonate complexes and their importance in actinide environmental chemistry, Chemical Reviews, v.95, pp. 25-48.

Finch, R. and T. Murakami (1999) Systematics and paragenesis of uranium minerals in: Uranium: Mineralogy, Geochemistry, and the Environment, Reviews in Mineralogy, V. 38, Mineralogical Society of America, Washington DC, Burns and Finch eds. pp. 91-180.

Fuller, C.C., J. Bargar, J. Davis, M. Piana, and M. Kohler (2002) Mechanisms of uranium interactions with hydroxyapatite: Implications for ground-water remediation. Environmental Science and Technology 36, 158-165.

Grenthe, I, J. Fuger, R.J.M. Konings, R.J. Lemire, A.B. Muller, C. Nguyen-Trung, and H. Wanner (1992) Chemical thermodynamics of uranium, Nuclear Energy Agency (NEA), North-Holland, 715 pp.

Kos, V. (1988) Modeling of uranium (IV) sorption and speciation in a natural sediment-groundwater system, Radiochimica ACTA, v.44/45, pp. 403-406.

Langmuir, D. (1997) Aqueous Environmental Geochemistry, Prentice-Hall, Upper Saddle River, NJ, 600 pp.

Langmuir, D. (1978) Uranium solution-mineral equilibria at low temperatures with applications to sedimentary ore deposits, Geochimica Et Cosmochimica Acta **V.** 42, 6, pp.547-569.

Meinrath, G., St. Fischer, K. Kohncke, and W. Voigt (1999) Solubility behavior of Uranium (VI) in alkaline solution, International Conference on Uranium Mining and Hydrogeology II, Freiburg, Germany, September 15-17, 1998, Abstracts and Programs.
Meinrath, G. (1998) Chemometric analysis: Uranium (VI) hydrolysis by UV-Vis spectroscopy, Journal of Alloys and Compounds 277: 777-781.

Meinrath, G. (1997) Chemometric and statistical analysis of U (VI) hydrolysis at elevated U (VI) concentrations, Radiochimica Acta 77(4): 221-234.

Millard, A. R. and R. E. M. Hedges (1996) A diffusion-adsorption model of uranium uptake by archaeological bone, Geochimica Et Cosmochimica Acta 60(12): 2139-2152.

Miyahara, K. (1993) Sensitivity of uranium solubility to variation of ligand concentrations in groundwater, Journal of Nuclear Science and Technology, v.30,n.4, pp. 314-332.

Murphy, E.L., and E.W. Shock (1999) Environmental aqueous chemistry of the actinides in: Uranium: Mineralogy, Geochemistry, and the Environment, Reviews in Mineralogy, V. 38, Mineralogical Society of America, Washington DC, Burns and Finch eds, pp. 221-254.

Ordonez-Regil E., R. Drot, and E. Simoni (2003) Surface complexation modeling of uranium (VI) onto lanthanum monophosphate, Journal of Colloid and Surface Science, In press.

Sowder, A. G., S. B. Clark, and R.A. Fjeld (2000) Dehydration of synthetic autunite hydrates. Radiochimica Acta 88(9-11): 533-538.

Sylwester, E. R., E. A. Hudson, et al. (2000) The structure of uranium (VI) sorption complexes on silica, alumina, and montmorillonite, Geochimica Et Cosmochimica Acta 64(14): 2431-2438.

Suzuki, S. and J.F. Banfield (1999) Geomicrobiology of uranium in: Uranium: Mineralogy, Geochemistry, and the Environment, Reviews in Mineralogy, V. 38, Mineralogical Society of America, Washington DC, Burns and Finch eds, pp. 393-492.

Taffet, M., V. Madrid, T. Carlsen, Z. Demir, J. Valett, M. Dresen, W. Daily, S. Coleman, V. Dibley, and L. Ferry (2004) Remedial Investigation/Feasibility Study for the Pit 7 Complex at Lawrence Livermore National Laboratory Site 300, Lawrence Livermore National Laboratory, Livermore, CA (UCRL-AR-202492) 96 pp.

United States Federal Register (2001) Maximum Contaminant Level for Uranium, Environmental Protection, U.S. Government Printing Office, Washington DC.

University of Washington (2002) The FEFF Project Documentation, Version 8.2, University of Washington, Department of Physics, Seattle, WA, 67 pp.

U.S. General Accounting Office (1998) Report to Congressional Requestors, Nuclear Waste-Understanding of Waste Migration is Inadequate for Key Decisions, U.S. General Accounting Office, Washington, D.C., 20548 (GAO/RCED-98-80 Nuclear Waste).

Valsami-Jones, E., K. V. Ragnarsdottir, A. Putnis, D. Bosbach, A.J. Kemp, and G. Cressey (1998) The dissolution of apatite in the presence of aqueous metal cations at pH 2-7, Chemical Geology 151(1-4): 215-233.

Figures

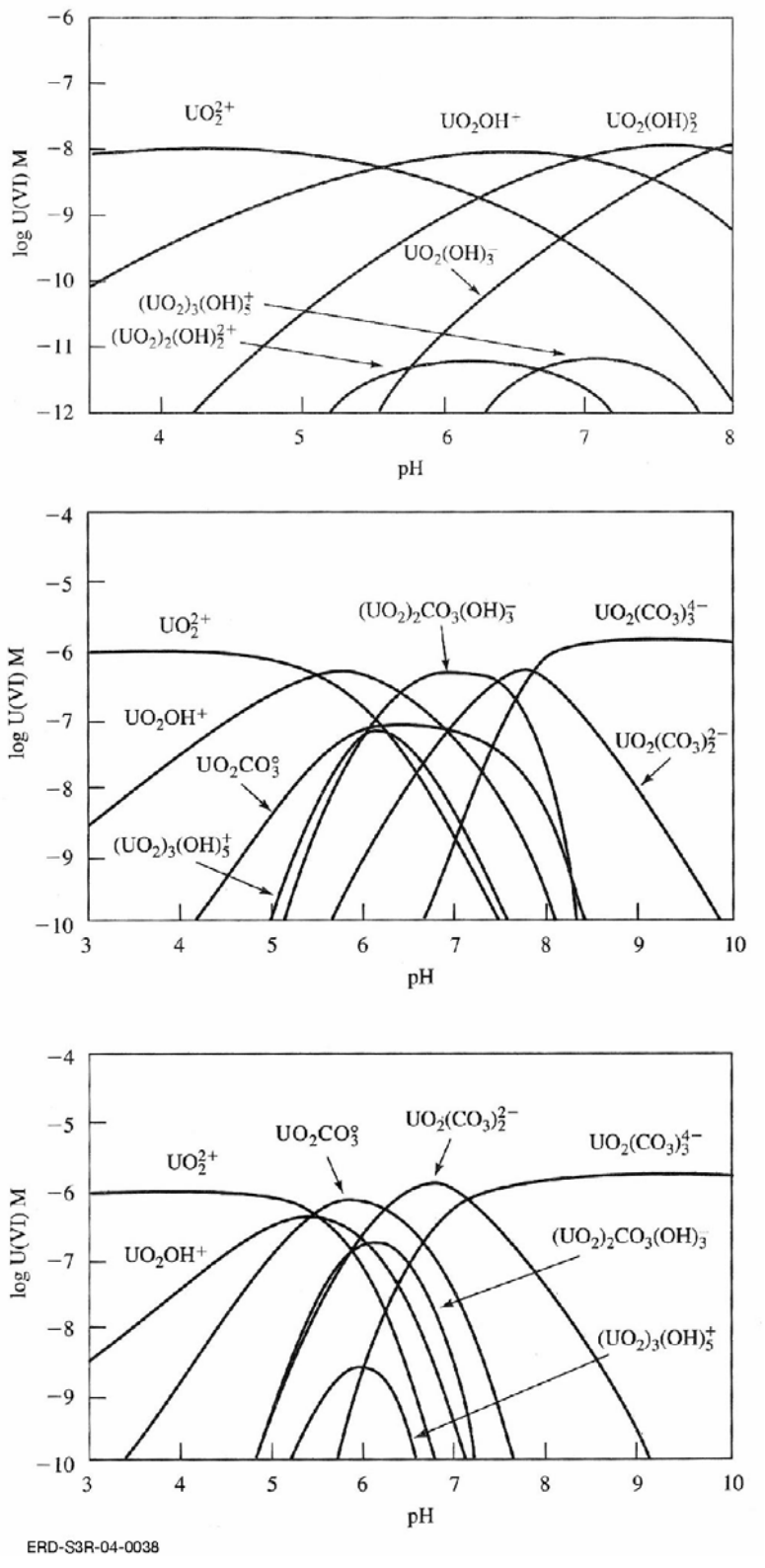

Figures 2.1a, b, and c. Distribution of U(VI) species at 25C and I = 0.1 for (a) U(VI) = 10^{-8} M and pCO_2 = 0 bar, (b) U(VI) = 10^{-6} M and pCO_2 = $10^{-3.5}$ bar, and (c) U(VI) = 10^{-6} M and pCO_2 = $10^{-2.0}$ bar (reprinted from Langmuir, 1997, Aqueous Environmental Chemistry).

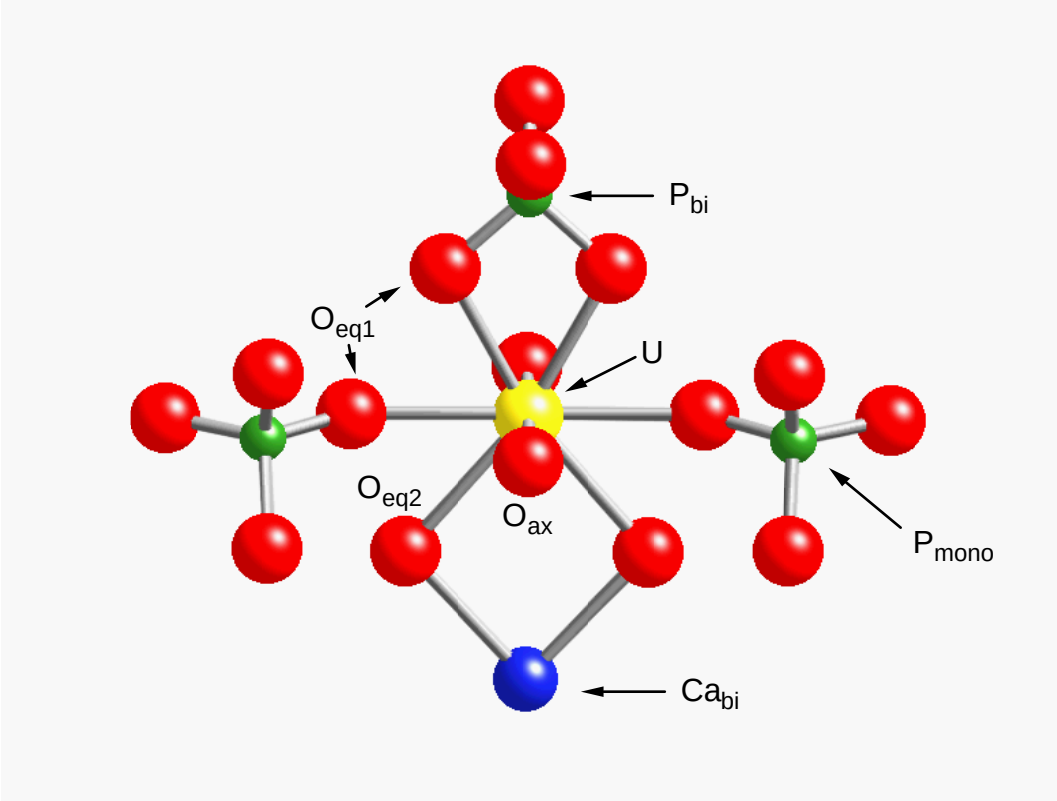

Figure 2.2. Uranium surface complexes that may occur on hydroxyapatite and that were verified by x ray absorption spectroscopy as part of this study. U = uranium, O_{eq1} = equatorial oxygen, O_{eq2} = equatorial oxygen, O_{ax} = axial oxygen, P_{bi} = bidentate phosphorus, P_{mono} = monodentate phosphorus, Ca_{bi} = bidentate calcium.

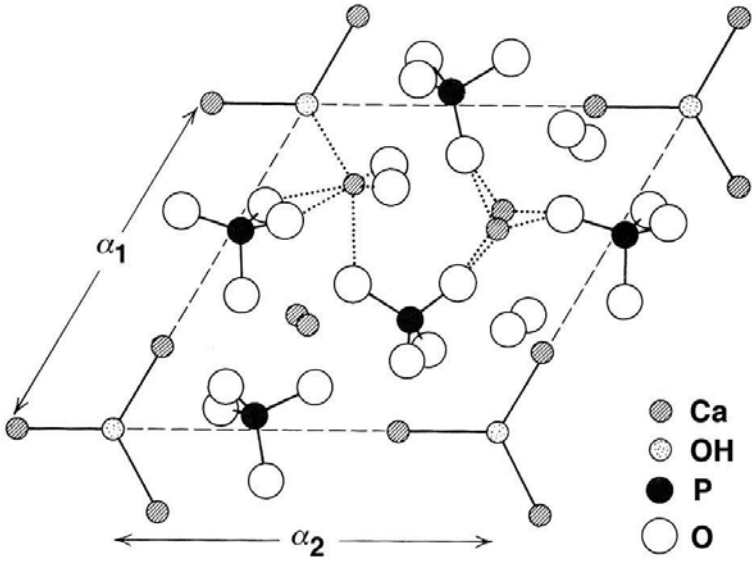

Figure 2.3. 0001 plane of the hydroxyapatite unit cell (reprinted from Hurlbut and Klein, 1988, Manual of Mineralogy).

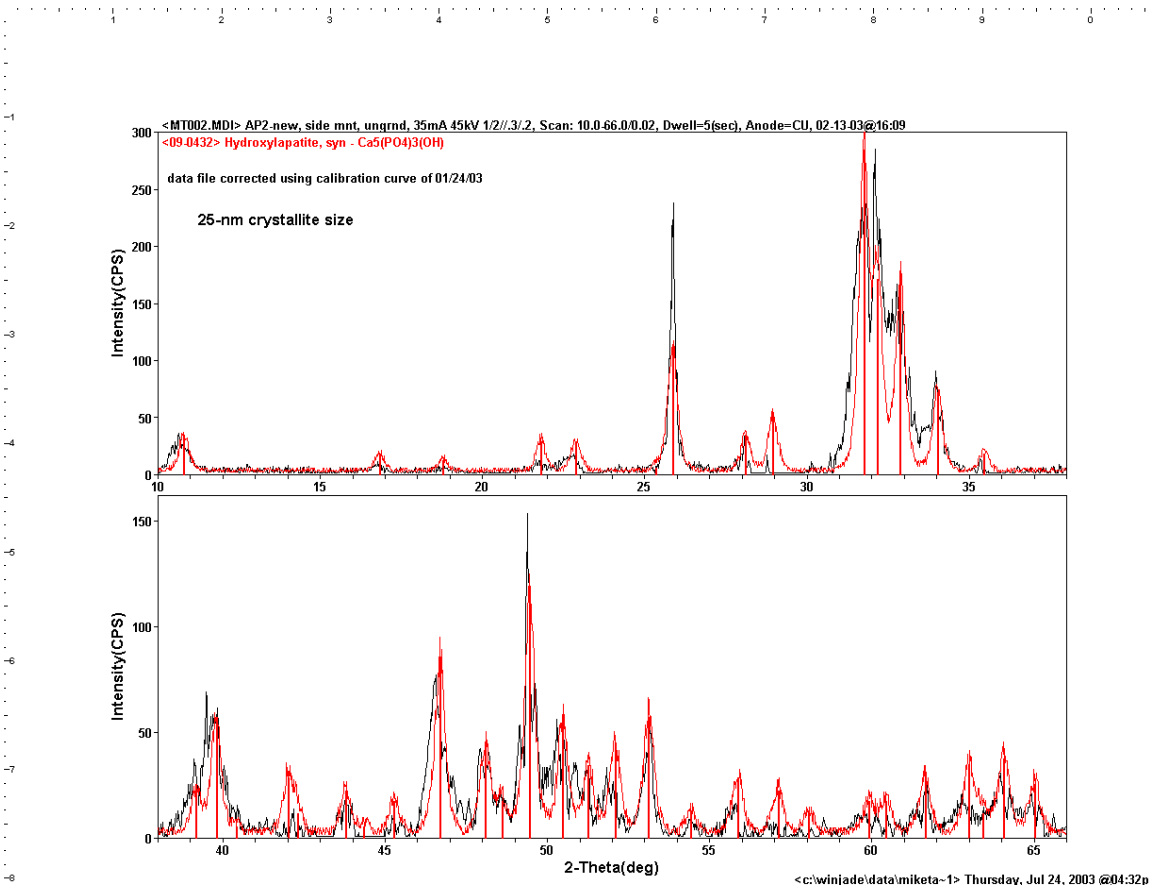

Figure 3.1. X-ray diffraction spectra for the crystalline hydroxyapatite used in the majority of the experiments. Red lines are reference curves for hydroxyapatite. Black lines are sample data.

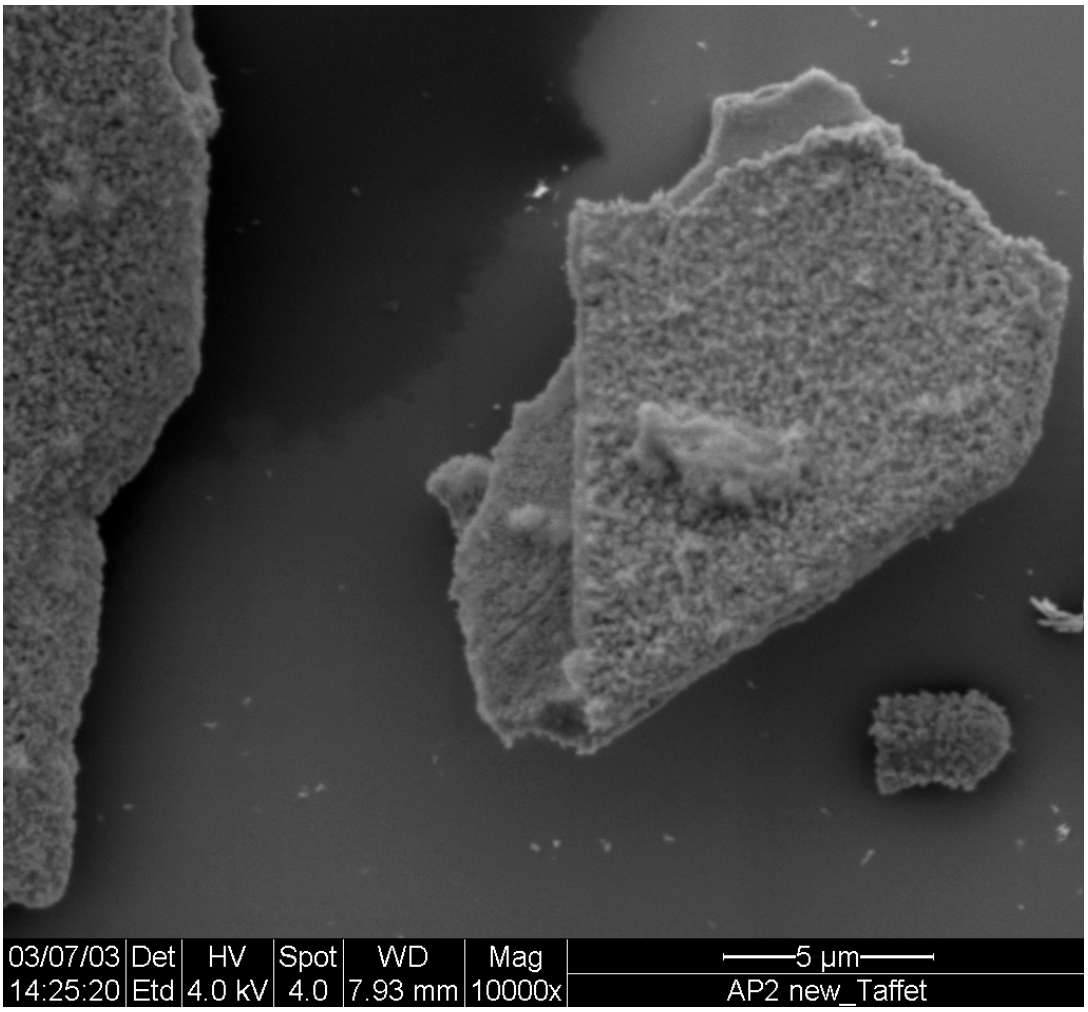

Figure 3.2. Crystalline hydroxyapatite (1000X magnification) showing nanocrystals averaging 25 nm in diameter.

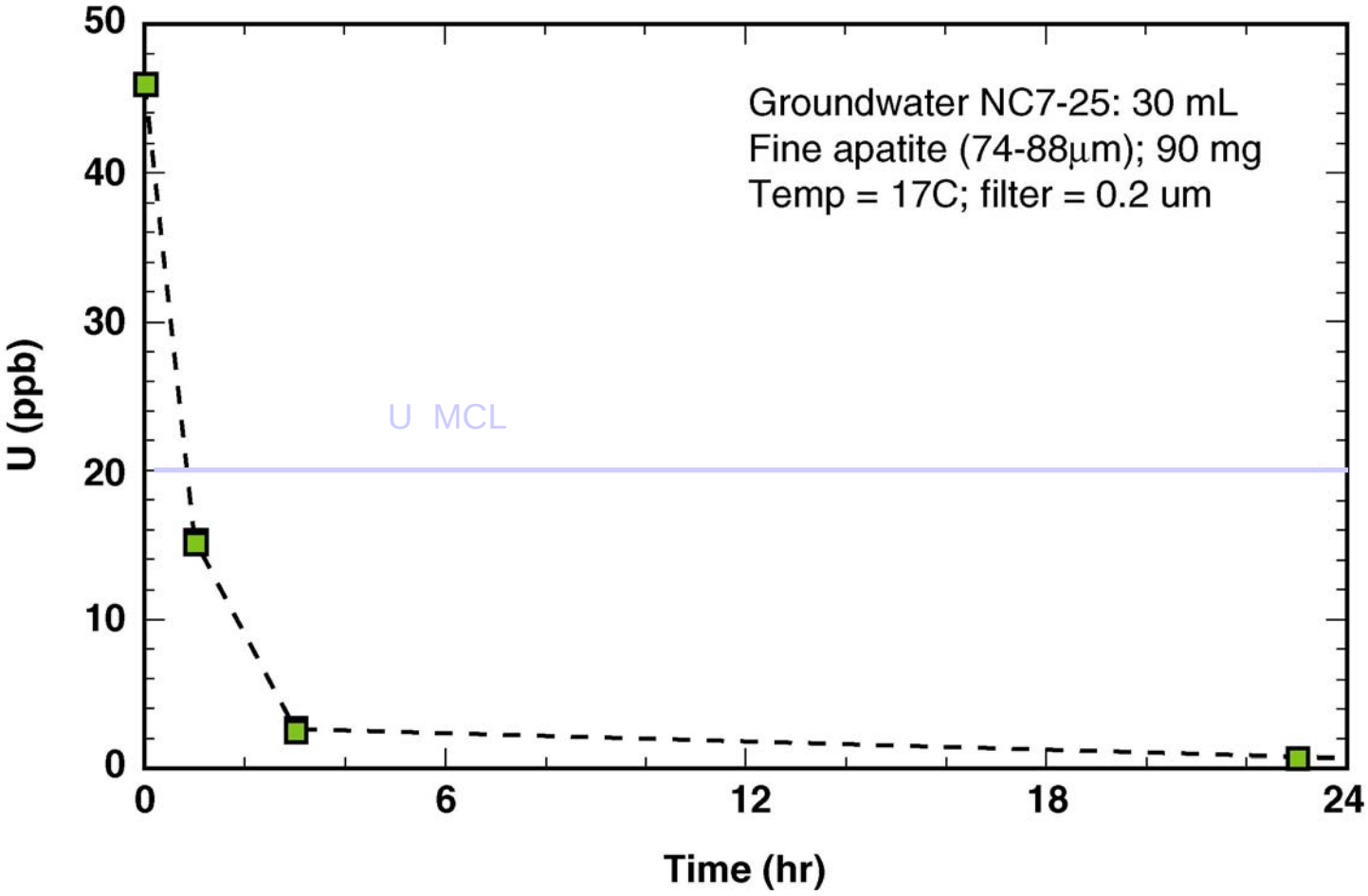

Figure 3.3. Reduction in dissolved uranium concentration with time in NC7-25 ground water reacted with fine fish bone at a 3:1000 solid:liquid ratio .

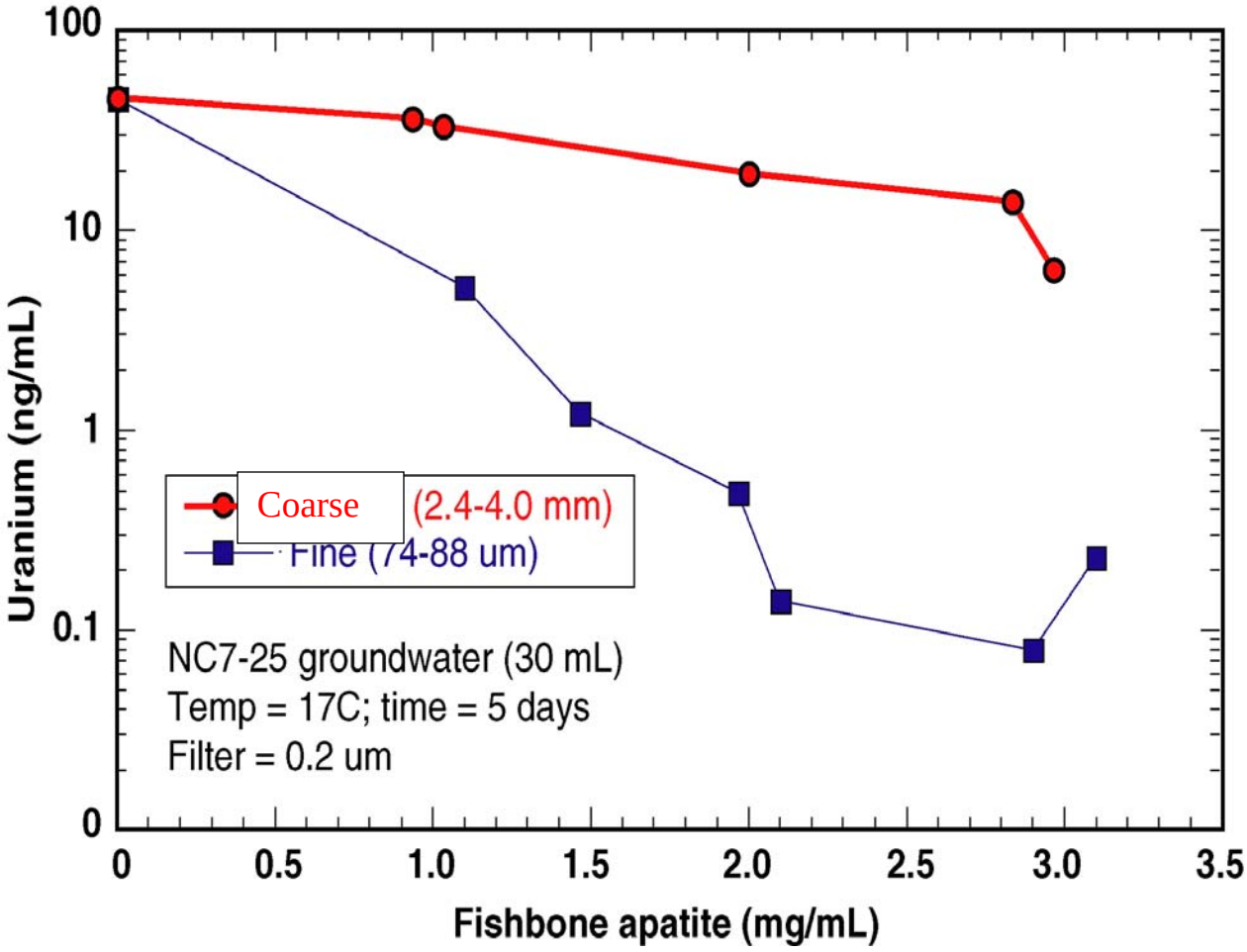

Figure 3.4. Dissolved uranium concentrations in ground water containing an initial uranium concentration of 45 ng/mL after 5 days reacting with several solid:liquid ratios and two size fractions of fish bone.

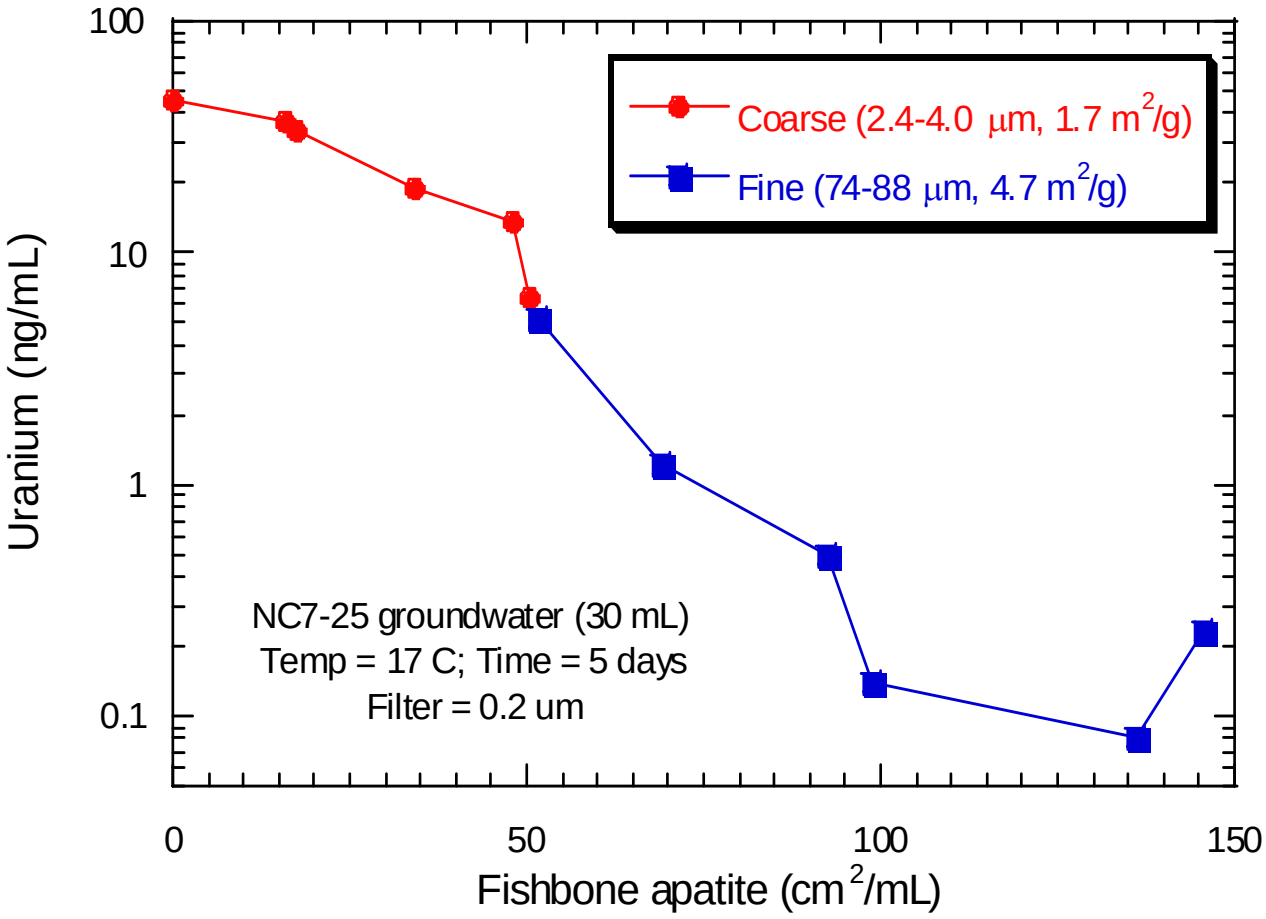

Figure 3.5. Dissolved uranium concentrations in ground water containing an initial uranium concentration of 45 ng/mL after 5 days of reaction with two size fractions of fish bone and several ratios of solid to liquid, plotted as a function of surface area per volume of solution.

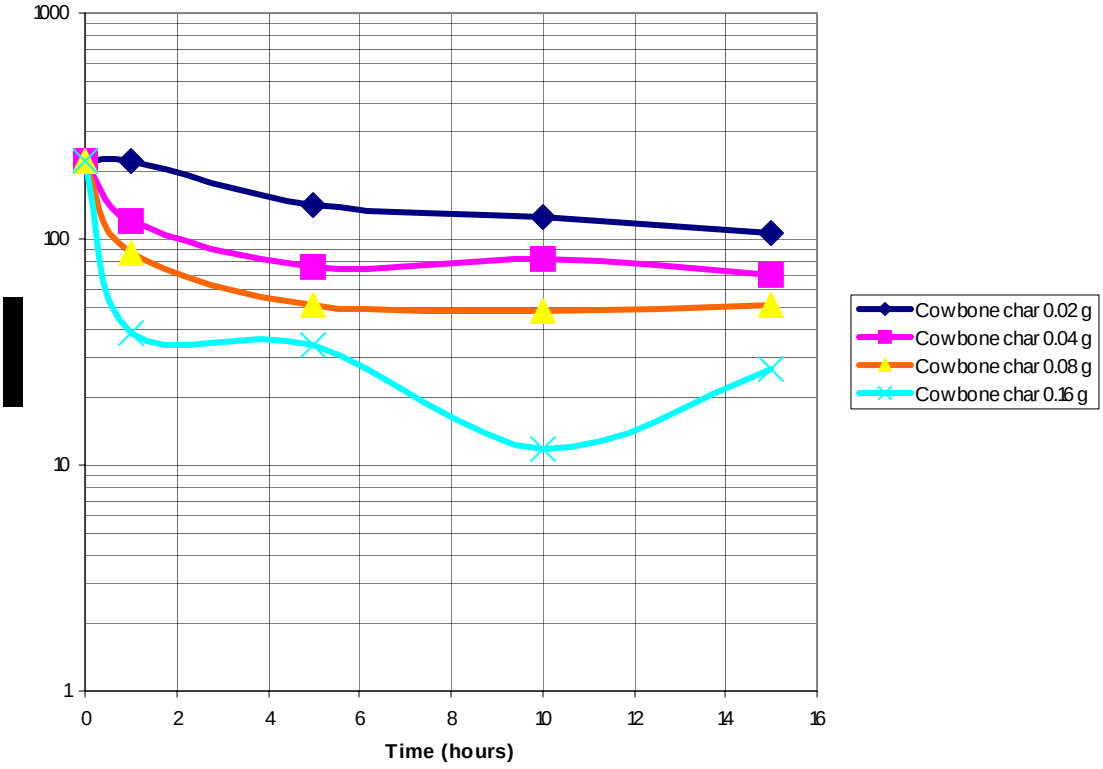

Figure 3.6. Plot of aqueous uranium concentration with time for four cow bone char solid:liquid ratios in 35 mL of NC7-40 ground water with an initial uranium concentration of 220.7 ng/mL.

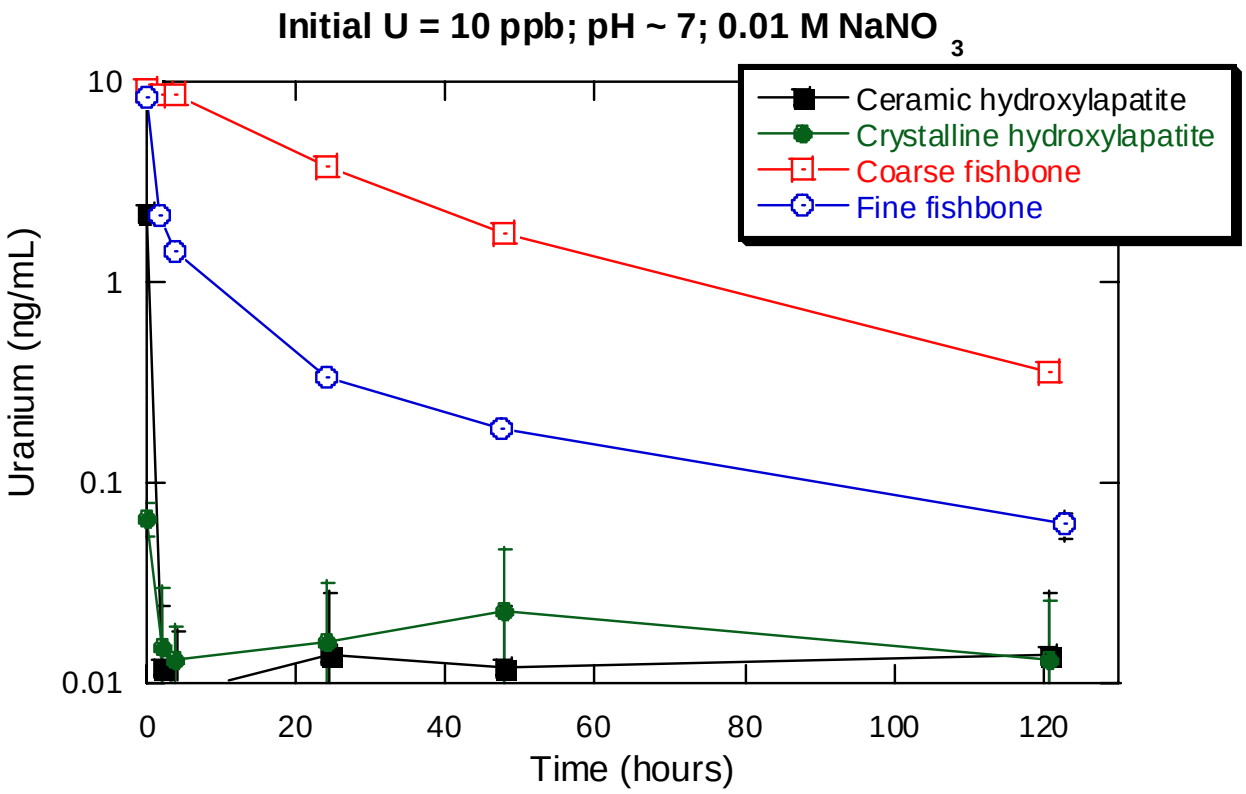

Figure 3.7. Dissolved uranium concentration with time for four hydroxyapatite forms reacted with pre-equilibrated 0.01 M $NaNO_3$ containing an initial uranium concentration of 10 ppb (ng/mL).

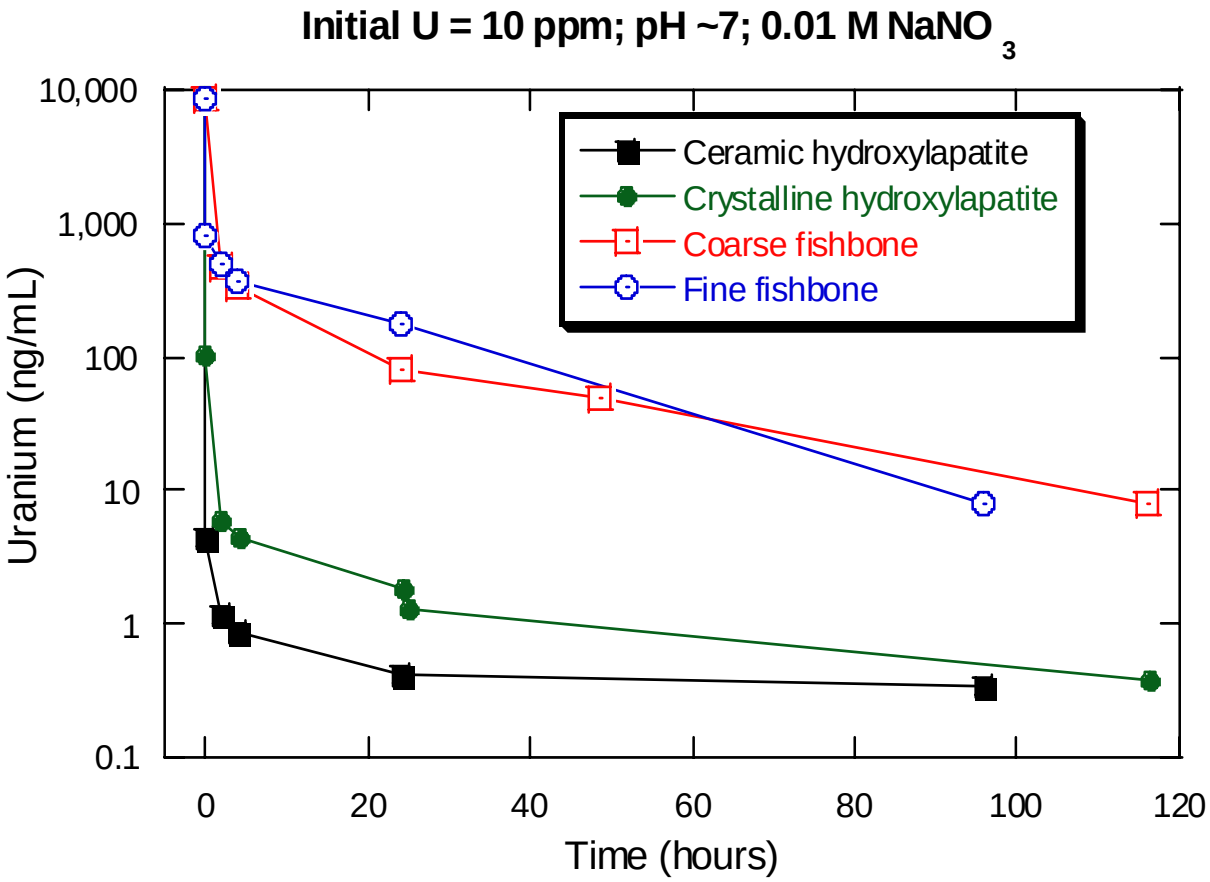

Figure 3.8. Dissolved uranium concentration with time for four hydroxyapatite forms reacted with pre-equilibrated 0.01 M $NaNO_3$ containing an initial uranium concentration of 10 ppm (μg/mL).

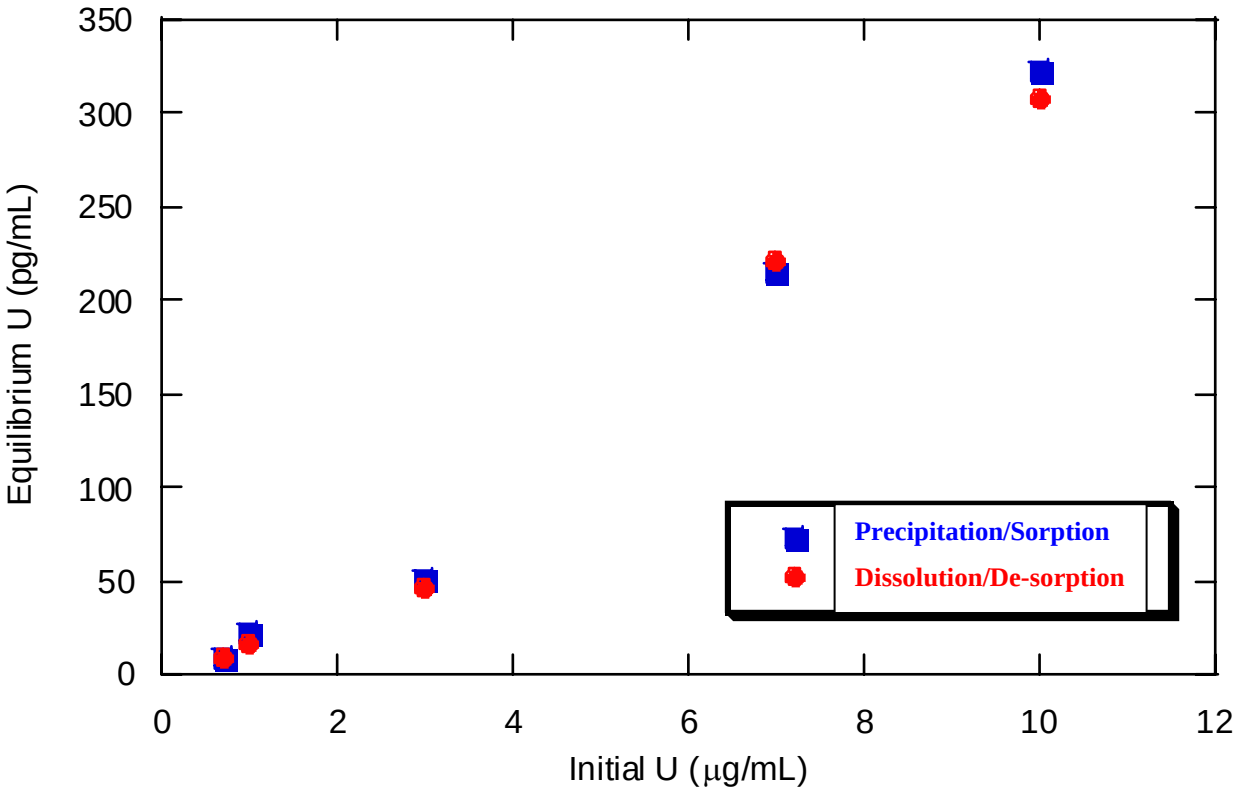

Figure 3.9. Dissolved uranium concentrations after 5 days of reaction of hydroxyapatite-equilibrated 0.01 M $NaNO_3$ (initial uranium concentration = 0.7 to 10 ppm) with hydroxyapatite (blue) and after 5 days of reaction of removed solid with uranium-free 0.01 M $NaNO_3$ (red).

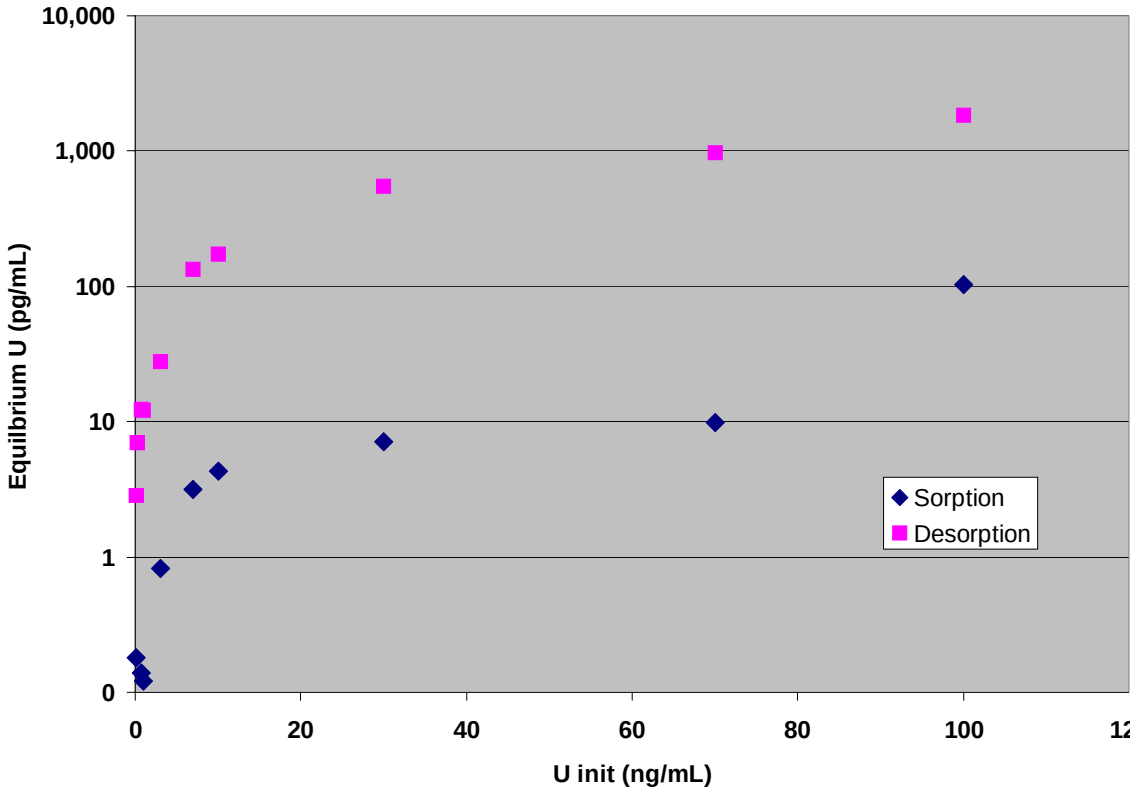

Figure 3.10. Dissolved uranium concentrations after 5 days of reaction of hydroxyapatite-equilibrated 0.01 M $NaNO_3$ (initial uranium concentration = 0.1 to 100 ppb [ng/mL]) with hydroxyapatite (blue) and after 5 days of reaction of removed solid with uranium-free 0.01 M $NaNO_3$ (purple).

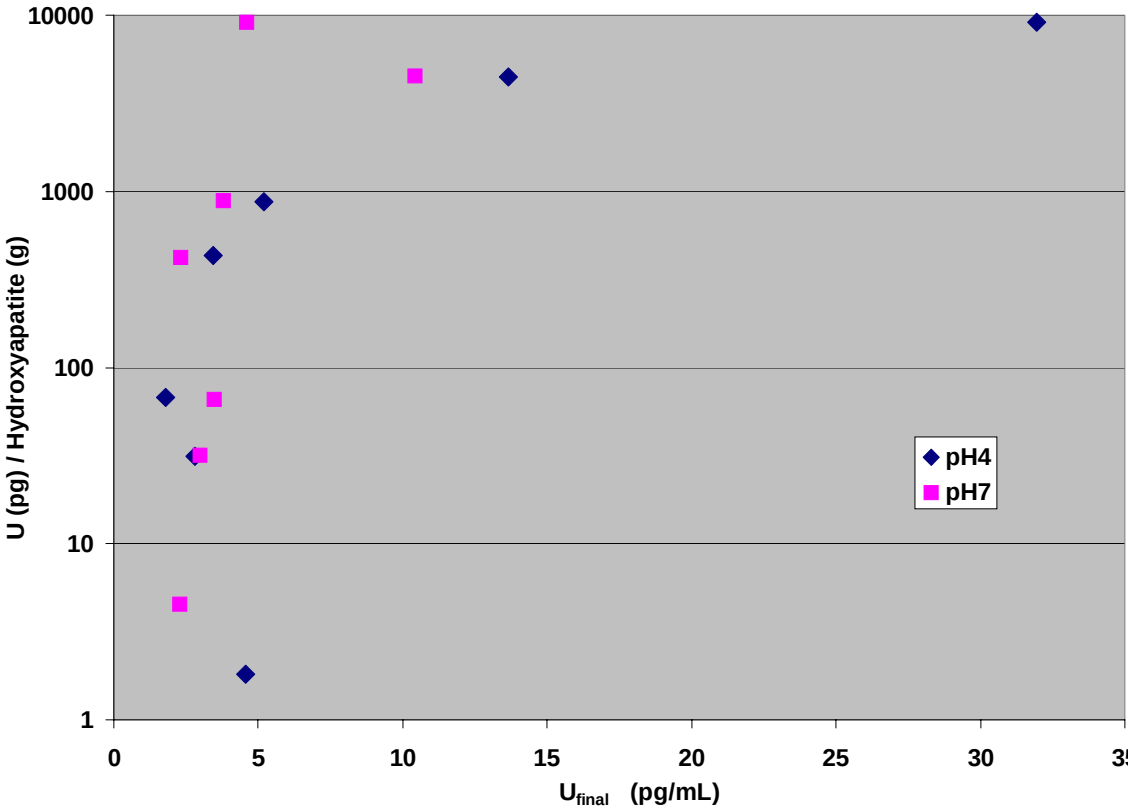

Figure 3.11. Isotherms showing sorbed uranium per gram of hydroxyapatite and steady-state aqueous uranium concentrations after 5 days of reaction for pH 4 and pH 7 experiments at initial uranium concentrations of 0.006 to 10 ppb (ng/mL).

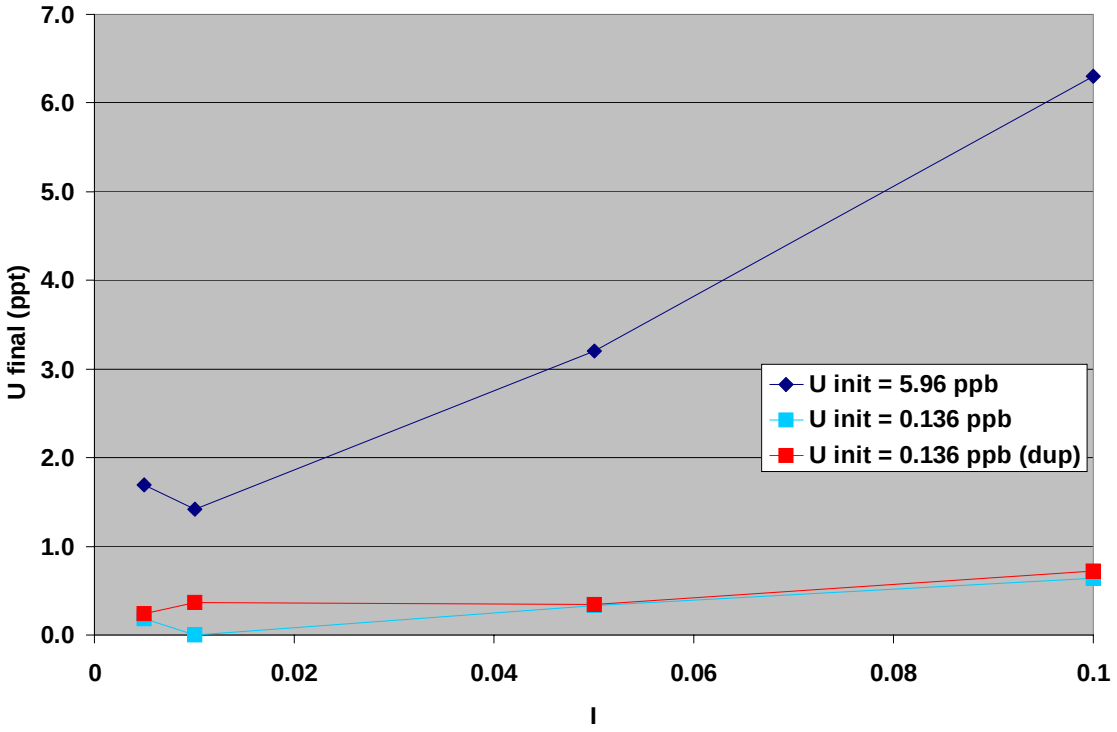

Figure 3.12. Steady-state dissolved uranium concentrations after 5 days of reaction of hydroxyapatite-equilibrated $NaNO_3$, at several different ionic strengths (I) and two initial uranium concentrations with hydroxyapatite.

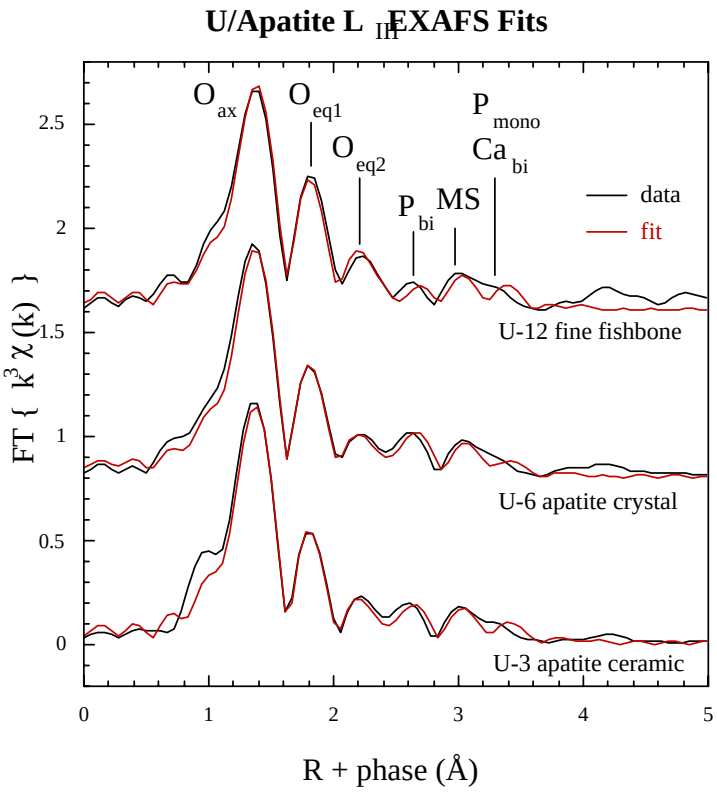

Figure 3.13. Uranium (U) L_{III} absorption edge extended x-ray adsorption fine structure data for three hydroxyapatite samples from batch experiments. Note: O_{ax} refers to peak for uranium (U) bound to axial oxygens (O), O_{eq1} and O_{eq2} to U bound to equatorial oxygens, P_{bi} to bidentate bonding of U to phosphorus (P), MS to multiple scattering due to axial oxygens, P_{mono} to monodentate bonding of U to P, and Ca_{bi} to bidentate bonding of uranium to calcium (Ca).

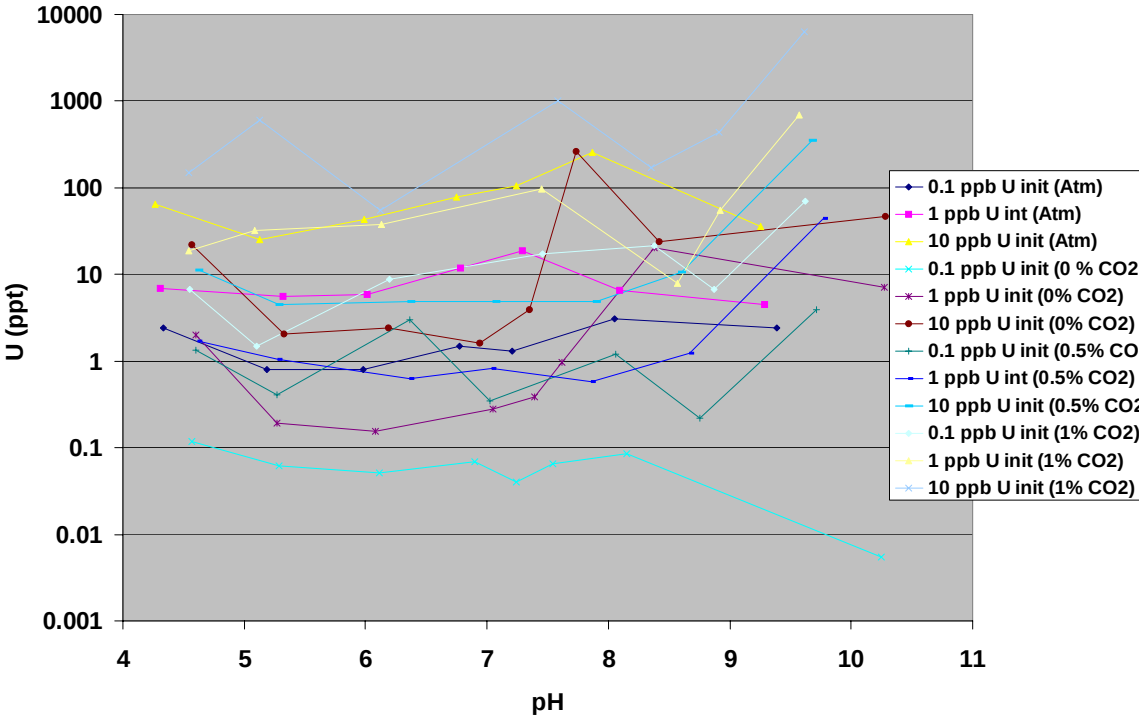

Figure 4.1 Summary of steady-state aqueous uranium concentrations for atmospheric, CO_2-free, 0.5% CO_2, and 1% CO_2 cases of hydroxyapatite reacted with pre-equilibrated $NaNO_3$ at pH 4 to 11 and initial uranium concentrations of 0.1, 1, and 10 ppb.

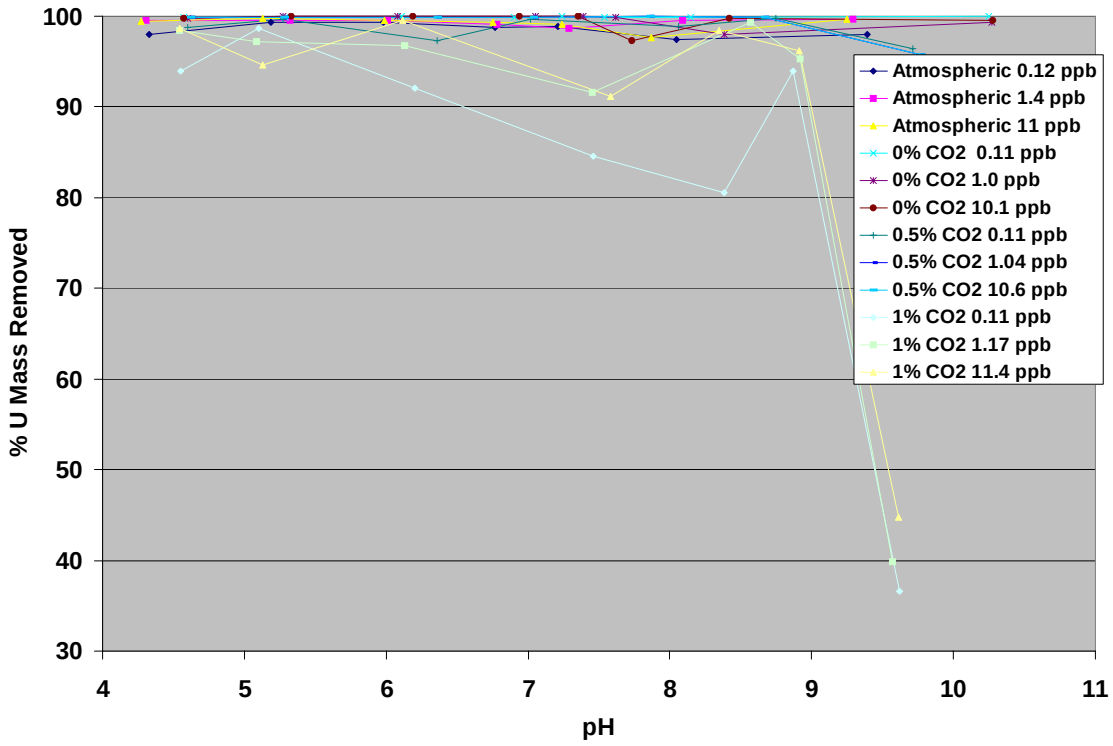

Figure 4.2 Summary of percentage of initial uranium concentrations removed by crystalline hydroxyapatite for atmospheric, CO_2-free, 0.5% CO_2, and 1% CO_2 cases of hydroxyapatite reacted with pre-equilibrated $NaNO_3$ at pH 4 to 11 and initial uranium concentrations of 0.1, 1, and 10 ppb.

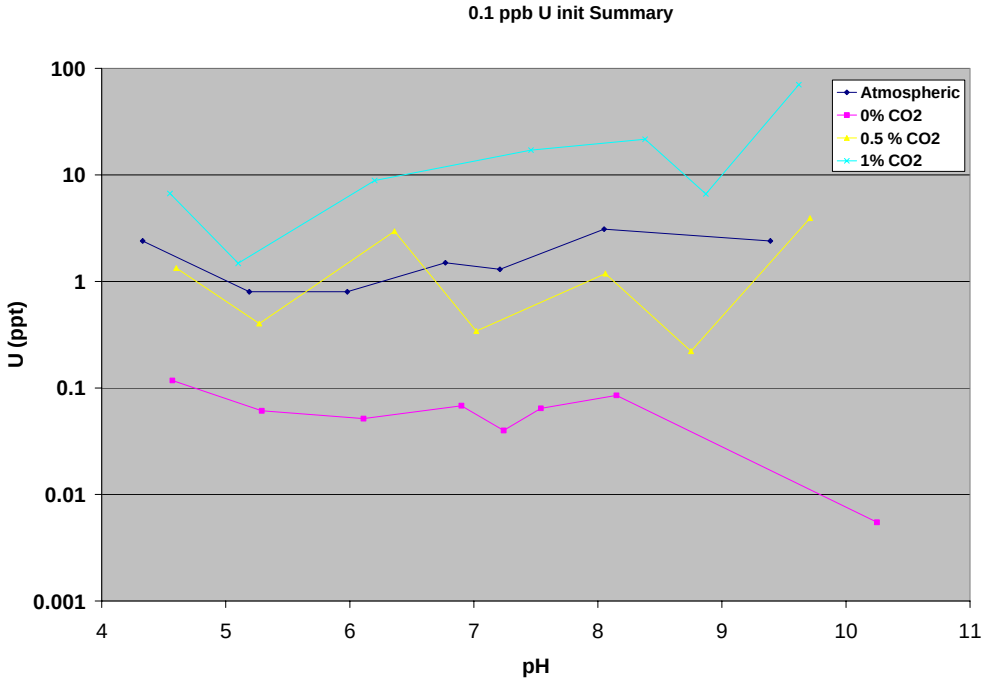

Figure 4.3. Steady-state aqueous uranium concentrations for atmospheric, CO_2-free, 0.5% CO_2, and 1% CO_2 cases of hydroxyapatite reacted with pre-equilibrated $NaNO_3$ at pH 4 to 10 and an initial uranium concentration of 0.1 ppb.

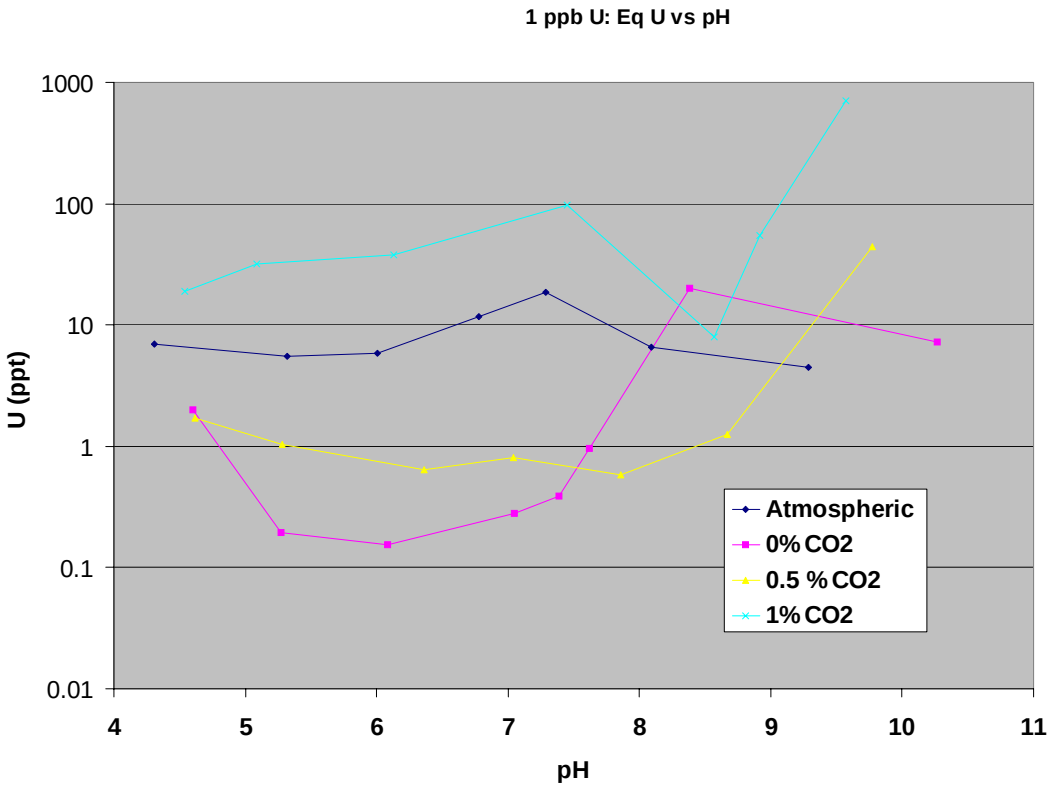

Figure 4.4. Steady-state aqueous uranium concentrations for atmospheric, CO_2-free, 0.5% CO_2, and 1% CO_2 cases of hydroxyapatite reacted with pre-equilibrated $NaNO_3$ at pH 4 to 10 and an initial uranium concentration of 1 ppb.

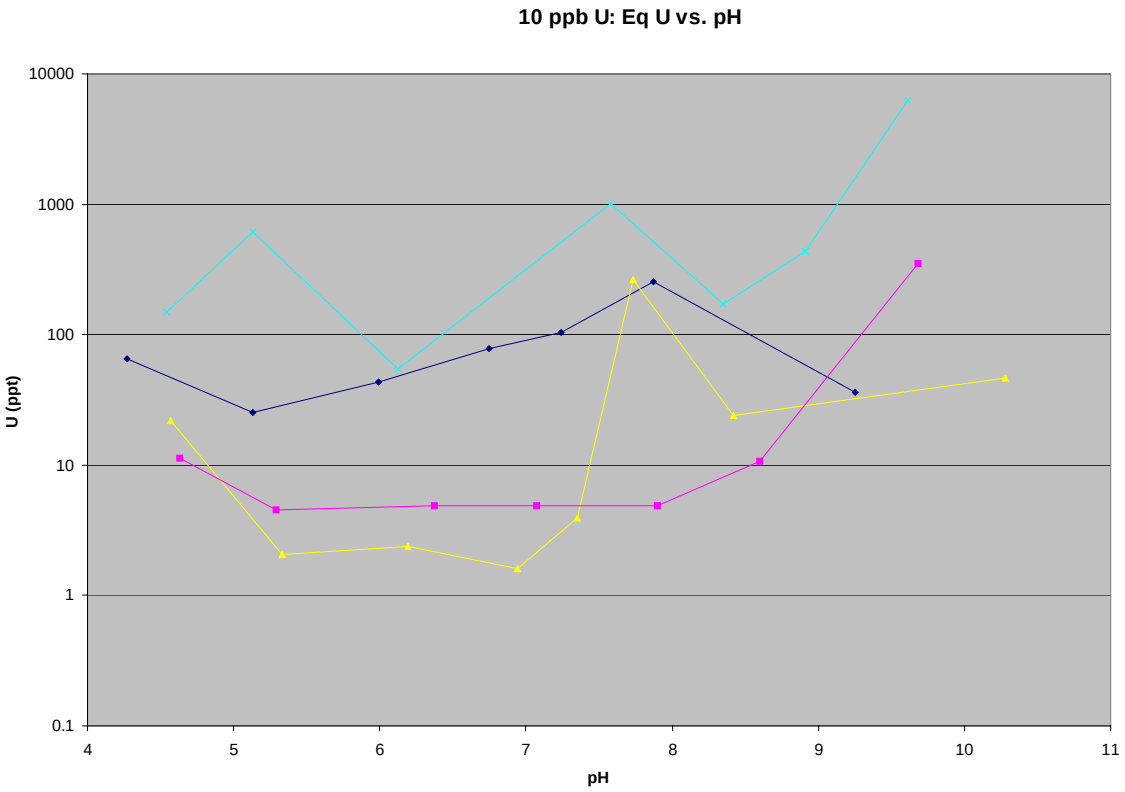

Figure 4.5. Steady-state aqueous uranium concentrations for atmospheric, CO_2-free, 0.5% CO_2, and 1% CO_2 cases of hydroxyapatite reacted with pre-equilibrated $NaNO_3$ at pH 4 to 10 and an initial uranium concentration of 10 ppb.

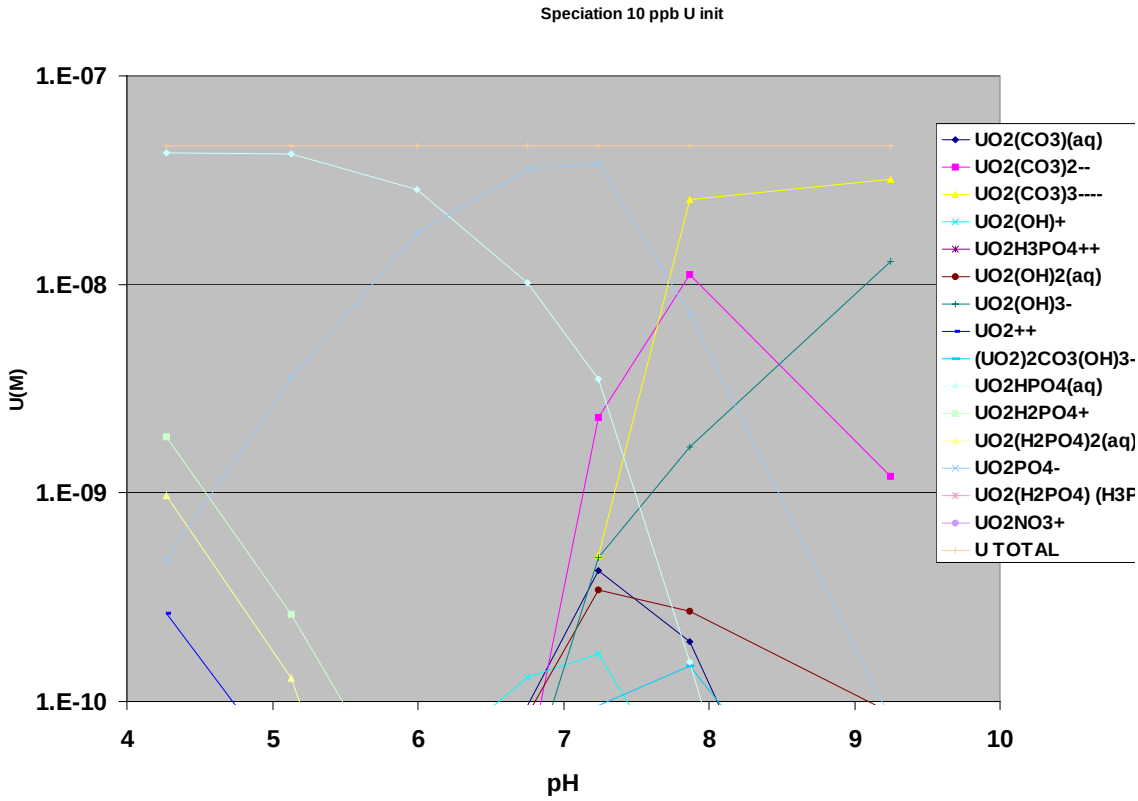

Figure 4.6. Aqueous uranium speciation for atmospheric CO_2 case at an initial uranium concentration of 10 ppb.

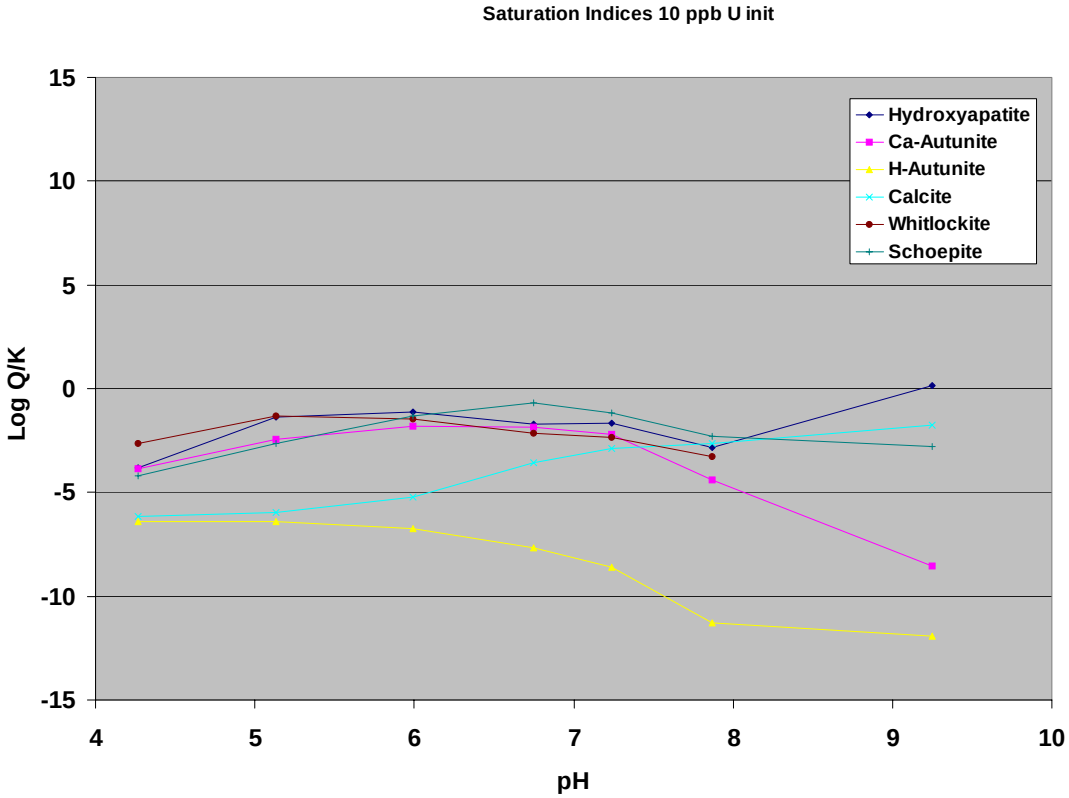

Figure 4.7. Mineral saturation indices for atmospheric CO_2 case at initial uranium concentration of 10 ppb.

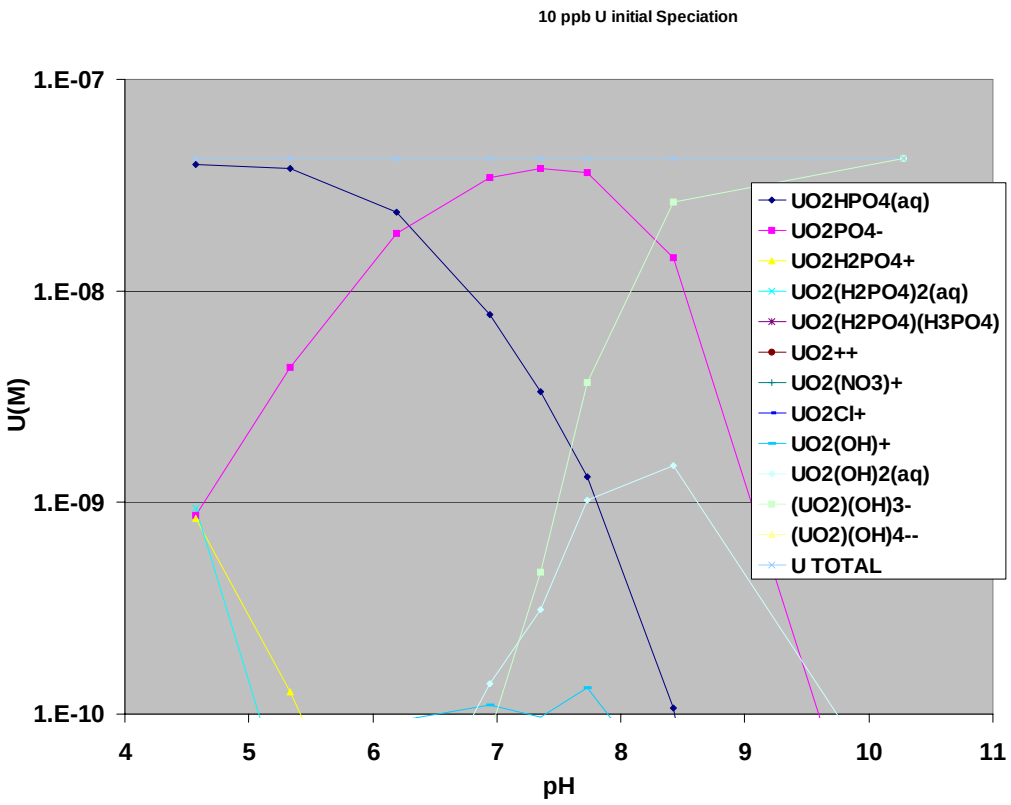

Figure 4.8. Uranium speciation for CO_2-free case at initial uranium concentration of 10 ppb.

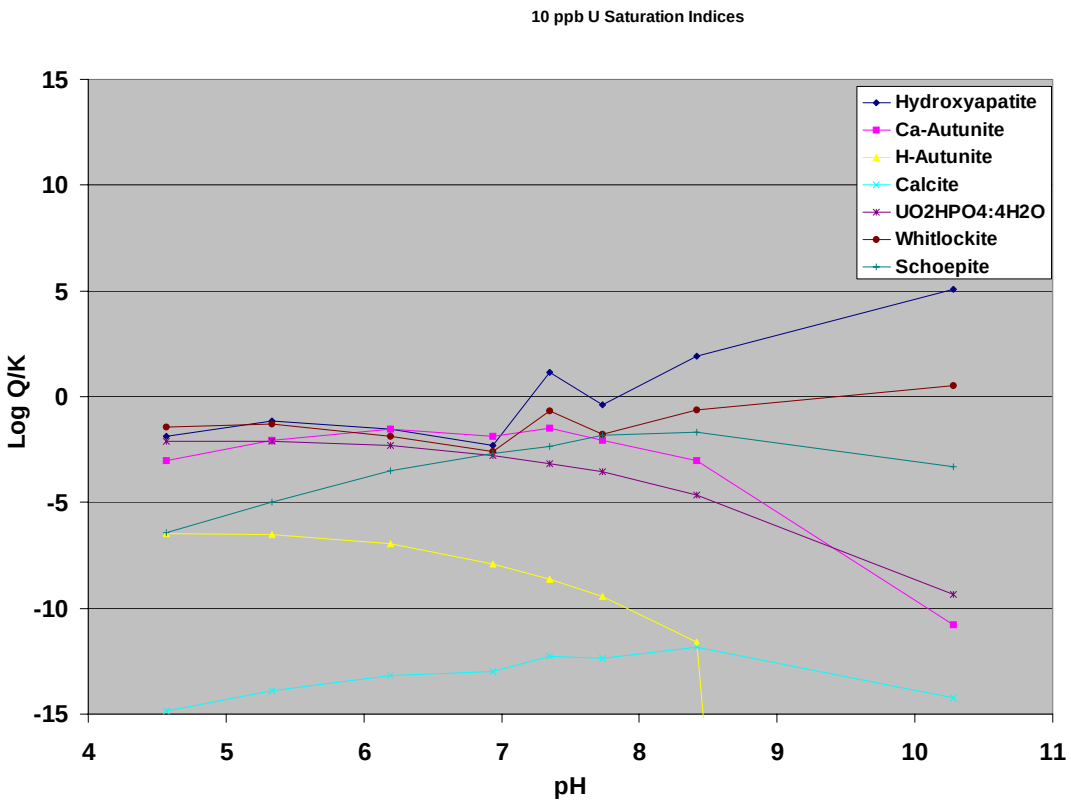

Figure 4.9. Mineral saturation indices for CO_2-free case at initial uranium concentration of 10 ppb.

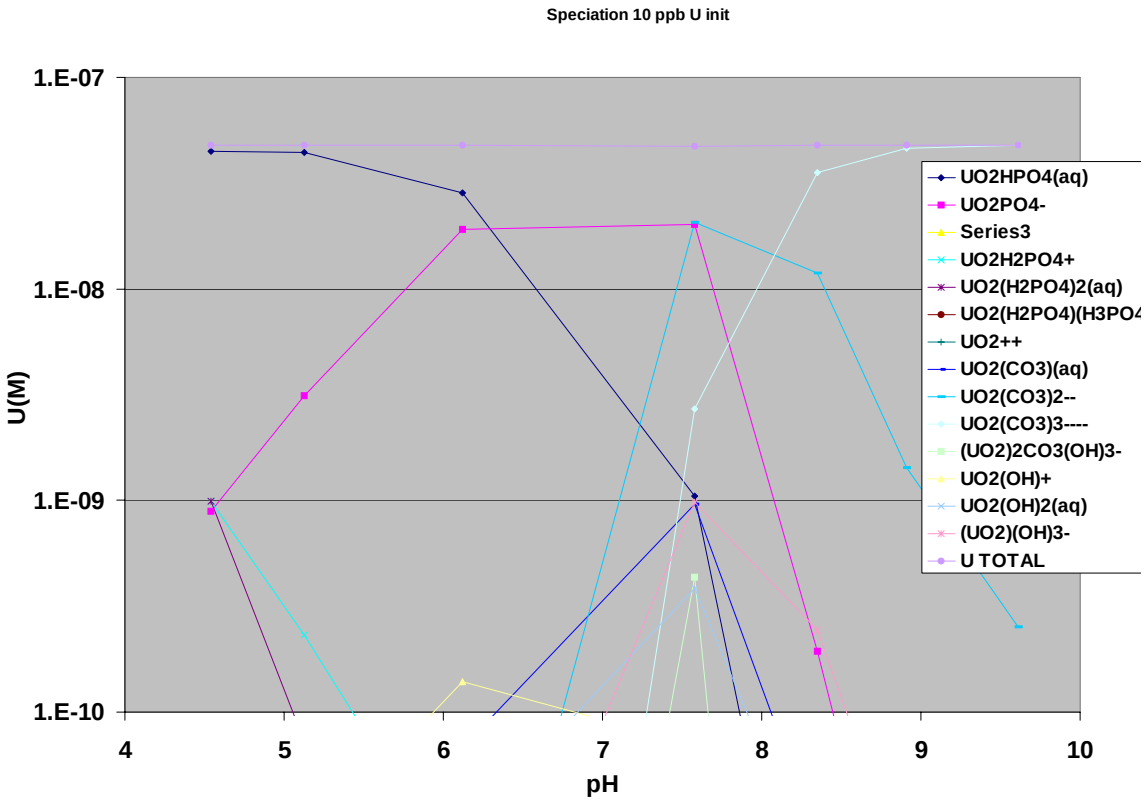

Figure 4.10. Uranium speciation for 1% CO_2 case at initial uranium concentration of 10 ppb.

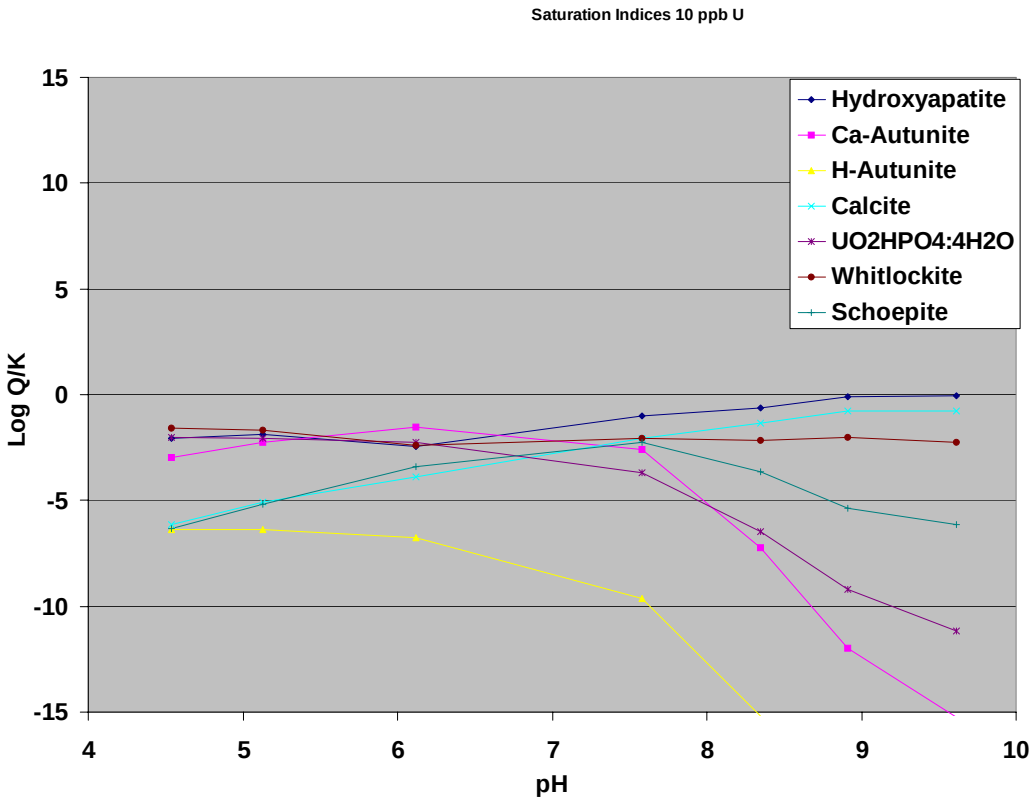

Figure 4.11. Mineral saturation indices for 1% CO_2 case at initial uranium concentration of 10 ppb.

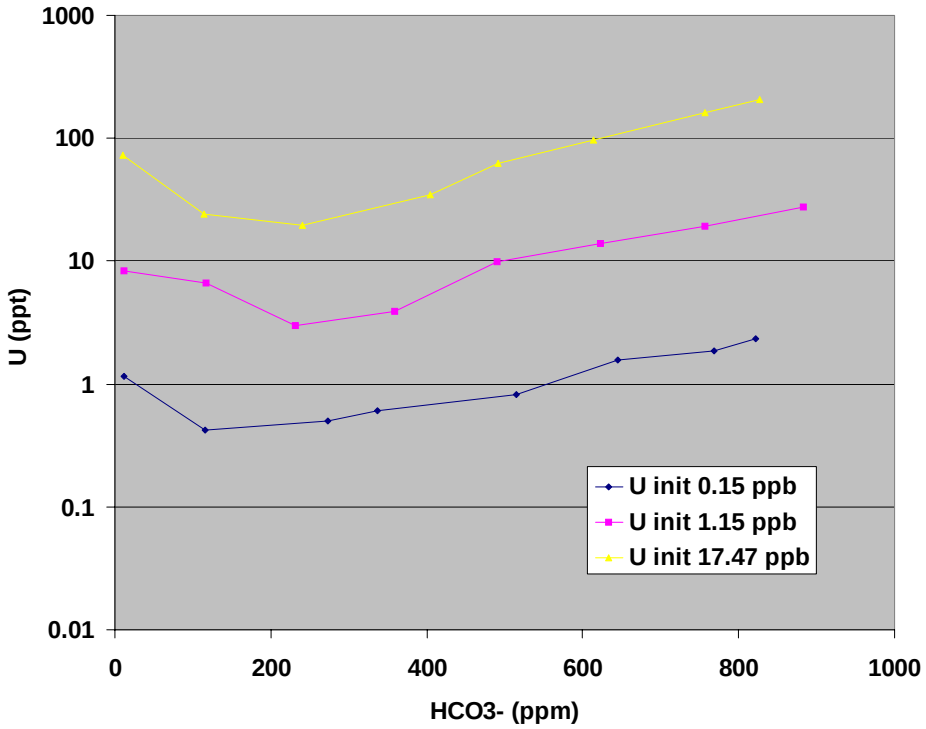

Figure 4.12. Steady-state aqueous uranium concentrations for a range of bicarbonate alkalinities and an initial uranium concentration of 10 ppb.

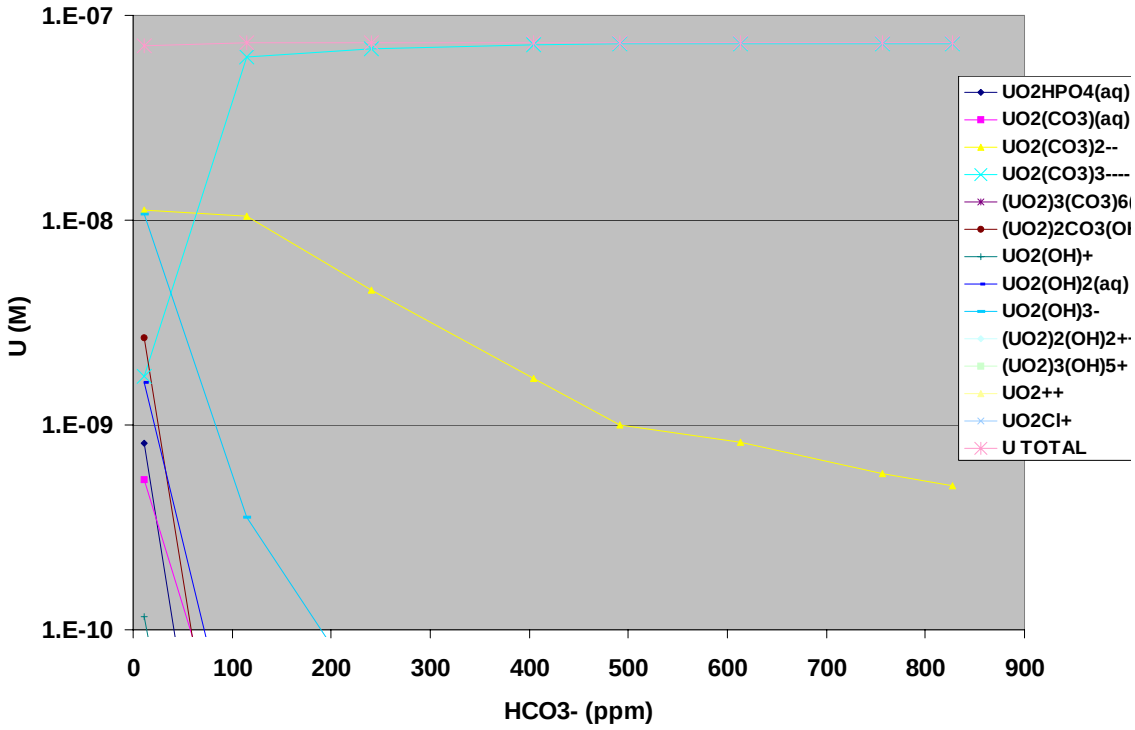

Figure 4.13. Uranium speciation for a range of bicarbonate alkalinities and an initial uranium concentration of 10 ppb.

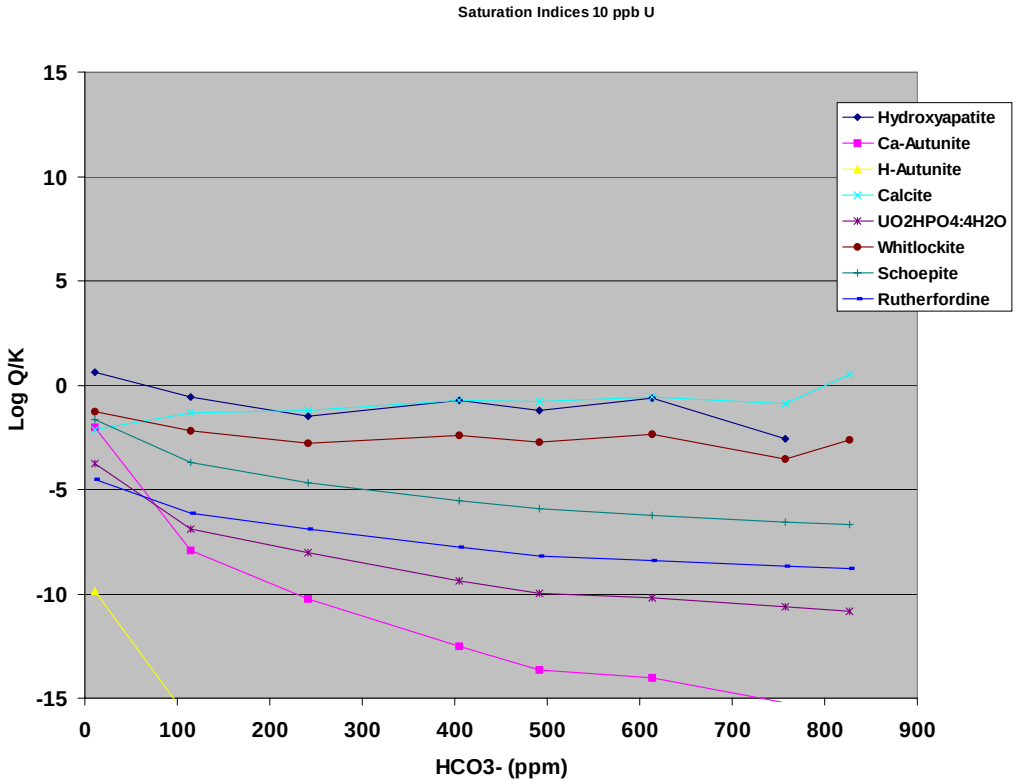

Figure 4.14. Mineral saturation indices for a range of bicarbonate alkalinities and an initial uranium concentration of 10 ppb.

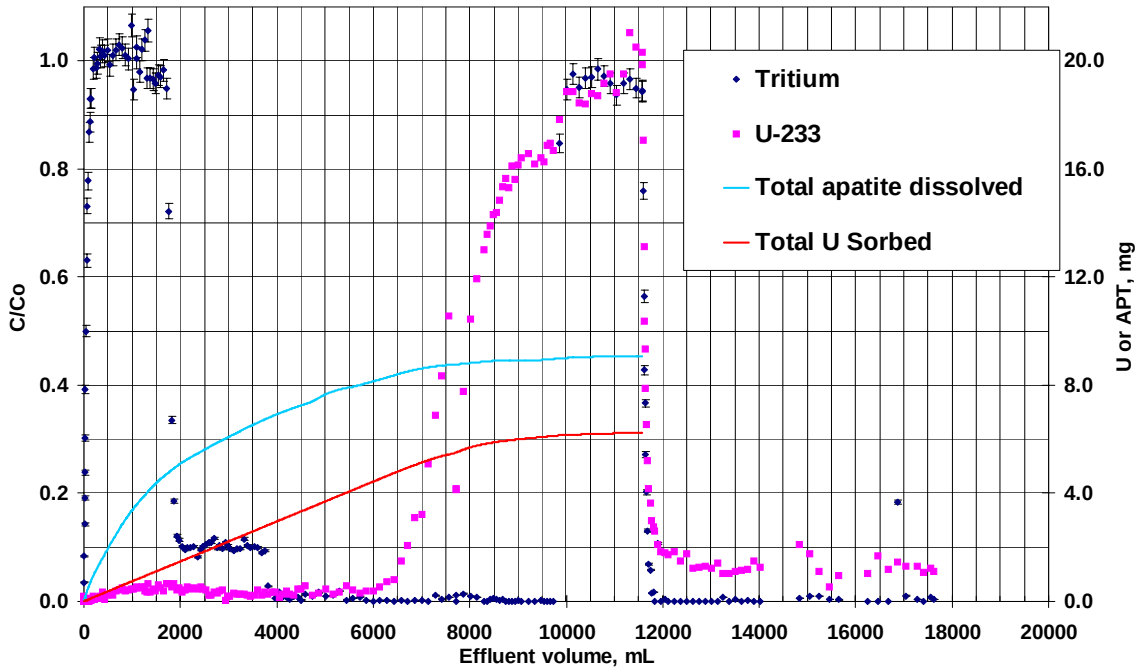

Figure 5.1. Details of hydroxyapatite stirred cell experiment with increasing effluent volume.

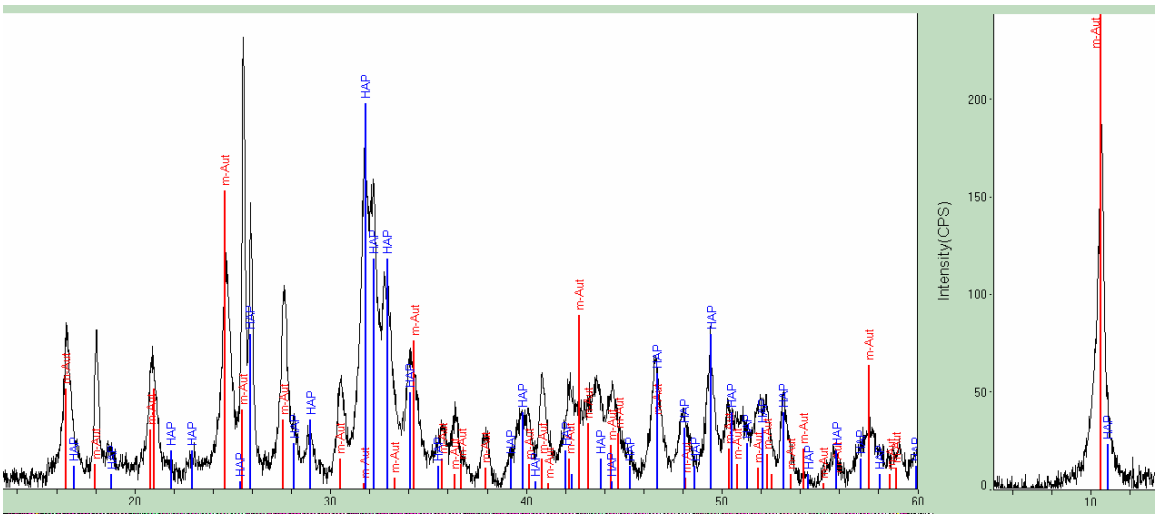

Figure 5.2. X ray diffraction spectra for hydroxyapatite collected at conclusion of stirred cell experiment showing hydroxyapatite (blue peaks) and meta-autunite (red peaks).

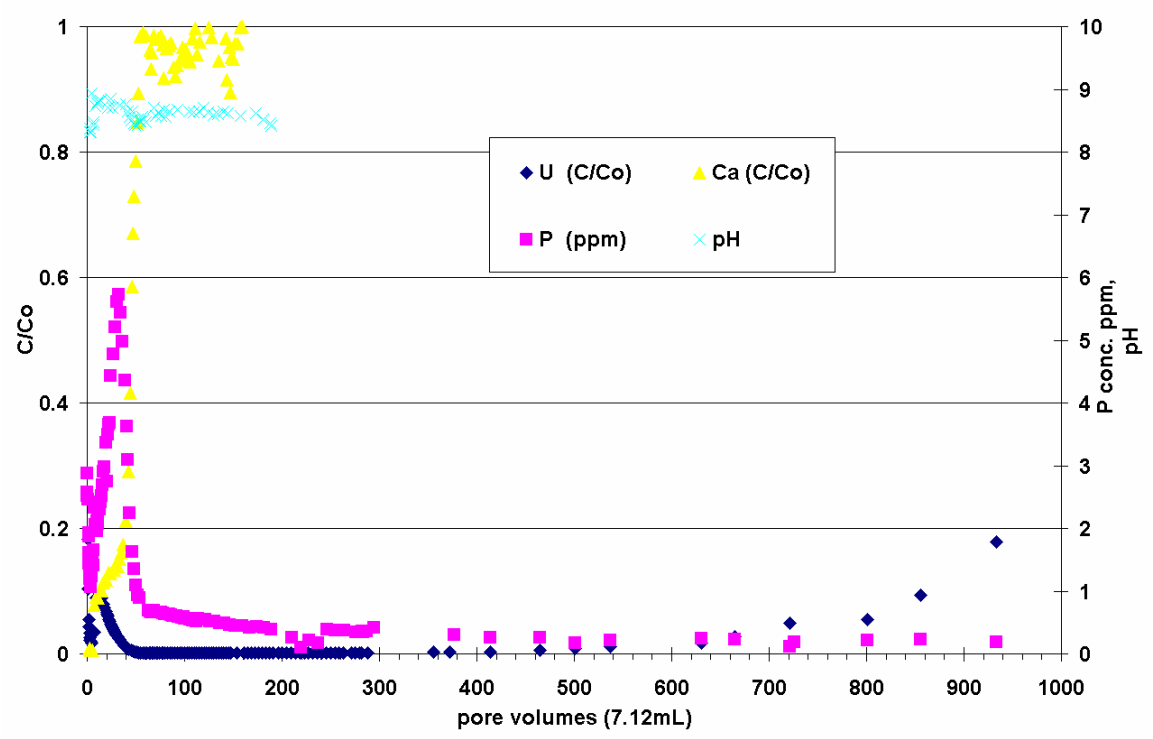

Figure 5.3. Results of column experiment with cow bone char and NC7-40 ground water containing about 260 ppb of uranium.

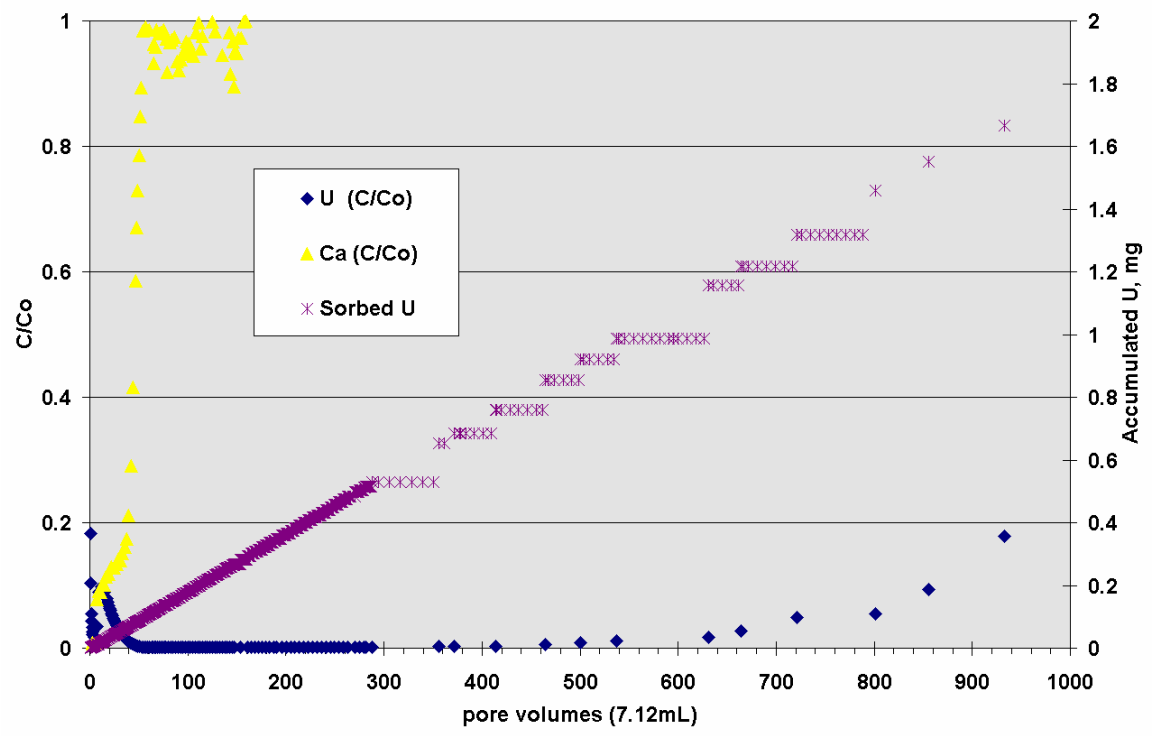

Figure 5.4. Results of column experiment with cow bone char and NC7-40 ground water containing about 260 ppb of uranium, showing accumulation of uranium on cow bone char.

Tables

Table 2.1 Solution equilibria for minerals relevant to this study.

$Ca_5(PO_4)_3(OH) + 4H^+ \leftrightarrow 3\ HPO_4^{-2} + 5\ Ca^{+2} + H_20$

Hydroxyapatite **log K_{eq} = -3.07**

$Ca_3(PO_4)_2 \leftrightarrow 3\ Ca^{+2} + 2\ HPO_4^{-2} - 2\ H^{+1}$

Whitlockite **lok K_{eq} =**

$2\ UO_2^{+2} + Ca^{+2} + 2\ HPO_4^{-2} + 10\ H_20 \leftrightarrow Ca(UO_2)_2(PO_4)_2 \bullet 10H_20 + 2H^+$

Calcium autunite **log K_{eq}= 20.06**

$2\ UO_2^{+2} + 2\ H^{+1} + 2\ HPO_4^{-2} + 10\ H_20 \leftrightarrow H_2(UO_2)_2(PO_4)_2 \bullet 10H_20 + 2H^+$

Hydrogen autunite **log K_{eq}= 23.75**

$UO_3{:}2H_2O \leftrightarrow UO_2 + 3\ H_20 - 2\ H^{+1}$

Schoepite **log K_{eq} = - 4.833**

$UO_2HPO_4{:}4H_20 \leftrightarrow UO_2 + HPO_4 + 4\ H_20$

$UO_2HPO_4{:}4H_2O$ **log K_{eq} = - 13.023**

Note: Data for calcium autunite, hydrogen autunite, and schoepite from Grenthe et al., 1992. All other data from Langmuir, 1997.

Table 3.1. Mean grain size and surface area of hydroxyapatite varieties used in this work.

Apatite	Grain Size (diameter)	Surface Area (m^2/g)
Ceramic hydroxyapatite	80 microns	42.0
Crystalline hydroxyapatite	80 microns	82.2
Fine fish bone	74-88 microns	4.7
Coarse fish bone	2.4- 4.0 mm	1.7
Cow bone char	0.51 mm	42.4